

# Geometry of the cumulant series in neuroimaging

Santiago Coelho,<sup>1</sup> Filip Szczepankiewicz,<sup>2</sup> Els Fieremans,<sup>1</sup> and Dmitry S. Novikov<sup>1</sup>

<sup>1</sup>*Center for Biomedical Imaging and Center for Advanced Imaging Innovation and Research (CAI<sup>2</sup>R),  
Department of Radiology, New York University School of Medicine, New York, USA*

<sup>2</sup>*Department of Medical Radiation Physics, Clinical Sciences Lund, Lund University, Lund, Sweden*

Water diffusion gives rise to micrometer-scale sensitivity of diffusion MRI (dMRI) to cellular-level tissue structure. The advent of precision medicine and quantitative imaging hinges on revealing the information content of dMRI, and providing its parsimonious basis- and hardware-independent “fingerprint”. Here we focus on the geometry of a multi-dimensional dMRI signal, classify all 21 invariants of diffusion and covariance tensors in terms of irreducible representations of the group of rotations, and relate them to tissue properties. Previously studied dMRI contrasts are expressed via 7 invariants, while the remaining 14 provide novel complementary information. We design acquisitions based on icosahedral vertices guaranteeing minimal number of measurements to determine 3–4 most used invariants in only 1–2 minutes for the whole brain. Representing dMRI signals via scalar invariant maps with definite symmetries will underpin machine learning classifiers of brain pathology, development, and aging, while fast protocols will enable translation of advanced dMRI into clinical practice.

## INTRODUCTION

Diffusion NMR or MRI (dMRI) measures a propagator of micrometer-scale displacements of water molecules in an NMR sample or an imaging voxel [1, 2]. Mapping its lowest-order cumulant, the voxel-wise diffusion tensor  $D$ , via diffusion tensor imaging (DTI) [3], has become an integral part of most human brain MRI clinical protocols and research studies. The information-rich signal beyond DTI forms the foundation of *tissue microstructure imaging* [4–10] — a combination of biophysics, condensed matter physics and bioengineering, that allows MRI to become specific to disease processes at the scale of cells and organelles, and to provide non-invasive markers of development, aging and pathology [2, 11, 12].

The information content of the dMRI signal depends on the degree of coarse-graining [5, 7] over the diffusion length controlled by the diffusion time  $t$ . With sufficiently long  $t \gtrsim 50$  ms used in the clinic, each *tissue compartment* (a non-exchanging water population, e.g., intra-axonal space, extra-axonal space, etc) can be asymptotically considered as fully coarse-grained, such that diffusion within it becomes Gaussian [5, 13, 14]. The signal  $S = \exp(-\text{tr}BD)$  (normalized to 1 in the absence of diffusion weighting) from any such “Gaussian compartment” defined by its diffusion tensor  $D$ , becomes fully encoded by a  $3 \times 3$  symmetric  $B$ -tensor [15–20]. The signal  $\langle S \rangle$  from a distribution of Gaussian compartments within a voxel is then represented by the cumulant expansion [19, 21, 22]

$$\ln \langle S \rangle = \ln \langle e^{-B_{ij}D_{ij}} \rangle = -B_{ij}D_{ij} + \frac{1}{2}B_{ij}B_{kl}C_{ijkl} + \mathcal{O}(b^3), \quad (1)$$

where  $b = \text{tr}B$  is the  $b$ -value, the summation over repeated Cartesian indices is assumed hereon, and

$$\begin{aligned} D_{ij} &= \langle D_{ij} \rangle, \\ C_{ijkl} &= \langle\langle D_{ij}D_{kl} \rangle\rangle \equiv \langle (D_{ij} - \langle D_{ij} \rangle)(D_{kl} - \langle D_{kl} \rangle) \rangle \end{aligned} \quad (2)$$

are the components of voxel-wise diffusion and covariance tensors  $D$  and  $C$ . Brackets  $\langle \dots \rangle$  denote averages over the distribution  $\mathcal{P}(D)$  of diffusion tensors characterizing tissue in a voxel (Fig. 1a), while  $\langle\langle \dots \rangle\rangle$  denote its cumulants [21]. Furthermore, the *time-dependent*  $\langle D_{ij}(t) \rangle$  and  $\langle\langle D_{ij}(t)D_{kl}(t) \rangle\rangle$

are relevant for shorter  $t$ , when compartmental diffusion is non-Gaussian (incomplete coarse-graining); they can be accessed [23, 24] with double diffusion encoding [18]. This makes understanding the tensors of the form (2) indispensable for dMRI.

A fundamental problem is to *classify symmetries* of the cumulant tensors (2) that are ubiquitous in representing a dMRI signal, and define their *tensor invariants*, i.e., basis-independent combinations of components (such as the trace  $D_{ii}$ ). With the advent of precision medicine and quantitative imaging [25], the invariants form a basis- and hardware-independent “fingerprint” of MRI signals [26–32]; their information content will underpin classifiers of pathology, development and aging [33]. A practical problem is to relate tensors and their invariants to tissue properties [4, 6], and to design fast unbiased measurements.

Here we study the geometry a dMRI signal by viewing the tensors (2) via the addition of “angular momenta” coming from the compartment tensors  $D$ . We decompose tensors  $D$  and  $C$  with respectively 6 and 21 degrees of freedom (dof) according to irreducible representations of the  $SO(3)$  group of rotations. We then construct and classify a complete set of  $3 + 18$  rotational invariants of the cumulant expansion (RICE) up to  $\mathcal{O}(b^2)$ . This reveals the cumulant tensors’ symmetries and geometric meaning, and connects with tissue biophysics embodied in the distribution  $\mathcal{P}(D)$ . We express all known dMRI contrasts up to  $\mathcal{O}(b^2)$  — mean diffusivity (MD), fractional anisotropy (FA), mean, radial and axial kurtosis (MK, RK, AK), microscopic FA ( $\mu$ FA), isotropic/anisotropic variance, etc — via just 7 RICE invariants. Besides uncovering 14 unexplored invariants, constructing RICE according to symmetries makes them maximally independent, and thus potentially more specific to tissue microstructure changes.

Our geometric approach applies to hundreds of thousands publicly available human dMRI brain datasets [34–39]. We also derive the shortest (“instant”) iRICE protocols for mapping MD, FA, MK in 1 minute, and MD, FA, MK,  $\mu$ FA in 2 minutes on a clinical scanner, making advanced dMRI clinically feasible. The methodology further applies to higher-order tensors in Eq. (1), as well as to the 4th-order elasticity tensor in materials science and geology [40–44].

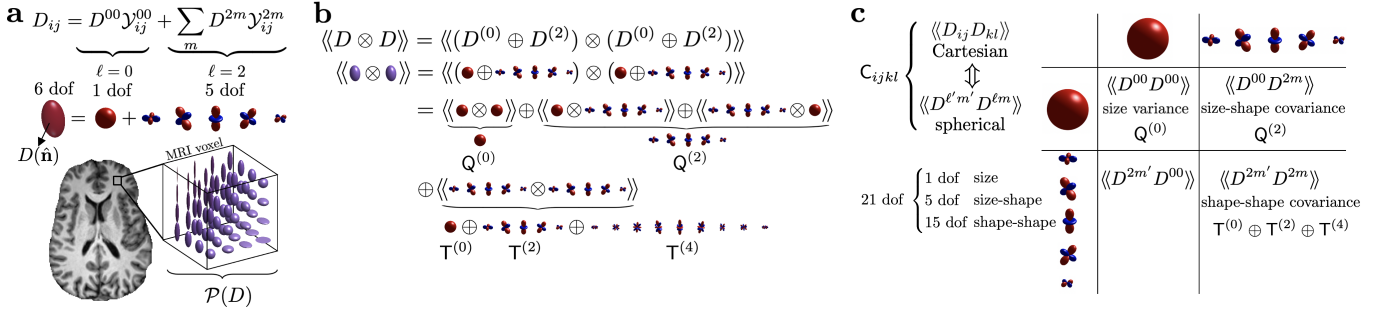


FIG. 1. Outline: (a) An MRI voxel as a distribution  $\mathcal{P}(D)$  of compartment diffusion tensors  $D$  decomposed in the spherical tensor basis. (b) The QT decomposition of the covariance tensor  $\mathbf{C}$  arises from the addition of “angular momenta”, Eq. (6): Central moments (2) of compartment tensors  $D$  correspond to tensor products, subsequently averaged over the voxel-wise distribution  $\mathcal{P}(D)$ . (c) Irreducible components of the QT decomposition represent 1 size-size, 5 size-shape, and 1 + 5 + 9 shape-shape covariances in the 21 dof of  $\mathbf{C}$ .

## RESULTS

### Warm-up: Irreducible decomposition of the diffusion tensor

Our main method of investigation will be the representation theory of the  $\text{SO}(3)$  group applied to cumulant tensors (2). To set the stage, recall that a  $3 \times 3$  symmetric matrix, such as a diffusion tensor  $D_{ij}$ , splits into an isotropic component,  $D_{ij}^{(0)}$ , and a symmetric trace-free (STF) component,  $D_{ij}^{(2)}$ :

$$D_{ij} = D_{ij}^{(0)} + D_{ij}^{(2)} = D^{00} \mathcal{Y}_{ij}^{00} + \sum_{m=-2}^2 D^{2m} \mathcal{Y}_{ij}^{2m}, \quad (3)$$

where the matrices  $\mathcal{Y}^{\ell m}$  form the standard spherical tensor basis, such that  $\mathcal{Y}^{\ell m}(\hat{\mathbf{n}}) = \mathcal{Y}_{ij}^{\ell m} n_i n_j$  are the spherical harmonics (SH) on a unit sphere  $|\hat{\mathbf{n}}| = 1$  [45]. Here we use the Racah normalization for SH (see *Materials and Methods*), such that  $\mathcal{Y}_{ij}^{00} = \delta_{ij}$  (unit matrix). The  $\ell = 0$  component is the mean diffusivity  $D^{00} = \frac{1}{3} \text{tr} D$  setting the overall size of the diffusion tensor ellipsoid  $D(\hat{\mathbf{n}}) = D_{ij} n_i n_j$ , while the five  $\ell = 2$  components  $D^{2m}$  are responsible for its shape and orientation.

Upon rotations, the spherical tensor components  $D^{\ell m}$  with different  $\ell$  do not mix:  $D^{2m}$  transform amongst themselves;  $D^{00}$  is an invariant. Mathematically, they belong to different irreducible representations of the  $\text{SO}(3)$  group [45–47]. Hence, Eq. (3) realizes the *irreducible decomposition*

$$D = D^{(0)} \oplus D^{(2)}, \quad D^{(\ell)} \equiv \{D^{\ell m}\}, \quad m = -\ell, \dots, \ell, \quad (4)$$

where each irreducible component of degree  $\ell$  has  $2\ell + 1$  dof, such that the 6 dof of a symmetric  $3 \times 3$  matrix  $D$  splits into  $6 = 1 + 5$ , cf. Fig. 1a. Spherical tensors will be our workhorse, as they represent high-dimensional objects using the minimal number of dof. Furthermore, irreducible components with different  $\ell$  point at distinct symmetries and physical origins.

The diffusion tensor in Eq. (3) may describe a microscopic tissue compartment. Consider the invariants of  $D$ : the ellipsoid’s shape is defined by 3 semi-axes (the eigenvalues). The remaining 3 dof define its orientation in space (e.g., 3 Euler’s angles), and depend on the coordinate frame. The irreducible

decomposition (4) allows one to construct tensor invariants symmetric with respect to the eigenvalues, and to assign the degree  $\ell$  to them. The simplest,  $\ell = 0$  invariant, is the trace  $\text{tr} D \propto D^{00}$ . The remaining two independent  $\ell = 2$  invariants are also given by traces:  $\text{tr}(D^{(2)})^2$  is proportional to the variance of the eigenvalues, and  $\text{tr}(D^{(2)})^3 = 3 \det D^{(2)}$  — to their product (readily seen in the eigenbasis of  $D^{(2)}$ ).

The overall diffusion tensor  $D_{ij}$  is the mean of the compartment tensors (3) over  $\mathcal{P}(D)$ , cf. Eq. (2). Invariants of  $D$  give rise to common DTI metrics, such as MD from  $\ell = 0$ ,

$$\text{MD} = D_0 \equiv D^{00} = \overline{D(\hat{\mathbf{n}})} = \frac{1}{3} D_{ii}, \quad (5)$$

and FA (from both  $\ell = 0$  and  $\ell = 2$  sectors, cf. Eq. (25) below). The 00 SH component equals the directional average (overbar) by virtue of the Racah normalization avoiding  $\sqrt{4\pi}$  factors.

The covariance tensor  $\mathbf{C}$  involves averages of the direct tensor products  $D \otimes D$ , Eq. (2). As such, it has a major symmetry (swapping first and second pairs of indices), and a minor symmetry (in each of the index pairs). Below we will formally map  $\mathbf{C}$  onto the addition of quantum angular momenta with  $\ell = 0$  or 2. This will allow us to construct all irreducible components of  $\mathbf{C}$  with distinct symmetries and geometric meaning, define all tensor invariants, reveal the redundancy in existing  $O(b^2)$  dMRI metrics and uncover 14 unexplored invariants, as well as relate the irreducible components to dMRI measurements and find ways of fast estimation of the most common invariants.

### Size and shape covariances: QT decomposition

Using the irreducible decomposition (4) in Eq. (2) results in

$$\begin{aligned} \mathbf{C} &= \langle\langle D \otimes D \rangle\rangle = \left\langle\left\langle \left( D^{(0)} \oplus D^{(2)} \right) \otimes \left( D^{(0)} \oplus D^{(2)} \right) \right\rangle\right\rangle \\ &= \mathbf{Q}^{(0)} \oplus \mathbf{Q}^{(2)} \oplus \mathbf{T}^{(0)} \oplus \mathbf{T}^{(2)} \oplus \mathbf{T}^{(4)}, \end{aligned} \quad (6)$$

where

$$\mathbf{Q}^{(0)} \equiv \left\langle\left\langle D^{(0)} \otimes D^{(0)} \right\rangle\right\rangle, \quad (7a)$$

$$\mathbf{Q}^{(2)} \equiv 2 \left\langle\left\langle D^{(0)} \otimes D^{(2)} \right\rangle\right\rangle, \quad (7b)$$

$$\mathbf{T} \equiv \left\langle\left\langle D^{(2)} \otimes D^{(2)} \right\rangle\right\rangle = \mathbf{T}^{(0)} \oplus \mathbf{T}^{(2)} \oplus \mathbf{T}^{(4)}. \quad (7c)$$

Formally, this corresponds to the addition of two quantum angular momenta with  $\ell = 0$  or  $\ell = 2$ , see graphical representation in Fig. 1b. As it is known from quantum mechanics [46], addition of angular momenta  $\vec{\ell}_1$  and  $\vec{\ell}_2$  yields all possible states with momenta  $\vec{\ell}$  between  $|\ell_1 - \ell_2|$  and  $\ell_1 + \ell_2$ . Mathematically speaking [47], the tensor product  $\vec{\ell}_1 \otimes \vec{\ell}_2$  of representations labeled by  $\ell_1$  and  $\ell_2$  is reducible, and splits into a direct sum of irreducible representations with  $\ell = |\ell_1 - \ell_2|, \dots, \ell_1 + \ell_2$ . Successive terms in Eq. (6) symbolically yield the representations with the following angular momenta, Eq. (7):  $\vec{0} \otimes \vec{0} = \vec{0}$ ;  $\vec{0} \otimes \vec{2} = \vec{2}$ ; and  $\vec{2} \otimes \vec{2} = \vec{0} \oplus \vec{2} \oplus \vec{4}$ . This yields the dof count for C tensor:  $21 = 1 + 5 + 1 + 5 + 9$ . In the  $\vec{2} \otimes \vec{2}$  case, the major symmetry of C ensures that the representations with  $\ell = 1$  and 3 do not contribute; they are forbidden by parity,  $(-1)^\ell = +1$ , based on the time-reversal invariance of the Brownian motion.

The physical intuition behind this formalism is as follows. In a distribution  $\mathcal{P}(D)$  of compartmental diffusion tensors of Fig. 1a, each ellipsoid (4) has an isotropic (“size”) part  $D^{(0)}$  and trace-free anisotropic (“shape”) part  $D^{(2)}$ . Thus, the direct products in Eq. (7) define the size variance  $Q^{(0)}$ , the size-shape covariance  $Q^{(2)}$ , and the shape-shape covariance T, Fig. 1b,c. The shape-shape covariance is reducible and further splits into three irreducible spherical tensors  $T^{(0)}$ ,  $T^{(2)}$  and  $T^{(4)}$ .

Besides the explicit classification based on symmetries, the benefit of using spherical tensors is in having the minimal number of dof in each of them, as compared to the highly redundant Cartesian objects such as  $C_{ijkl}$ . Therefore, one expects that the covariances  $\langle\langle D^{\ell_1 m_1} D^{\ell_2 m_2} \rangle\rangle$  of the spherical-tensor components (4) of compartmental diffusivities should be related to the corresponding spherical-tensor components of Q and T, Fig. 1c. We derive these explicit relations based on the spherical tensor algebra in Supplementary Section S2. In brief, the relations for Q,

$$Q^{00} = \langle\langle (D^{00})^2 \rangle\rangle, \quad Q^{2m} = 2 \langle\langle D^{00} D^{2m} \rangle\rangle, \quad (8a)$$

follow trivially from Eqs. (7a) and (7b). However, Eq. (7c)

$$T^{\ell m} = \langle 2020 | \ell 0 \rangle \sum_{m_1+m_2=m} \langle 2m_1 2m_2 | \ell m \rangle \langle\langle D^{2m_1} D^{2m_2} \rangle\rangle \quad (8b)$$

involves the Clebsch-Gordan coefficients [46]  $\langle \ell_1 m_1 \ell_2 m_2 | \ell m \rangle$  which obey the selection rule  $m_1 + m_2 = m$  and vanish otherwise. This rule makes the system (8) so sparse that it can be inverted by hand, cf. Supplementary Eq. (S16). This provides an analytical solution for the tissue properties  $\langle\langle D^{\ell_1 m_1} D^{\ell_2 m_2} \rangle\rangle$  in terms of the spherical components of T and Q, i.e., the irreducible components of covariance tensor C. We call Eqs. (6)–(8) the *QT decomposition* of covariance tensor.

#### Q and T tensor components from B-tensor shells

The rank of the B tensor reflects how many dimensions of the diffusion process are being probed simultaneously; rank B > 1 means probing the diffusion along more than one dimension. An example is the axially symmetric family [20, 48]

$$B_{ij}(b, \beta, \hat{\mathbf{g}}) = b \left( \beta g_i g_j + \frac{1-\beta}{3} \delta_{ij} \right) \quad (9)$$

parametrized by its trace  $b$  setting the overall scale; by the unit vector  $\hat{\mathbf{g}}$  along the symmetry axis; and by shape parameter  $\beta$ .

Historically, diffusion weightings in MR have mostly probed a single direction  $\hat{\mathbf{g}}$  per measurement, using pulsed gradients [49], such that  $B_{ij} = b g_i g_j$ ; this so-called linear tensor encoding (LTE,  $\beta = 1$ ) corresponds to rank B = 1. Varying  $\beta$  changes the B-tensor shape, e.g.,  $\beta = 0$  for spherical tensor encoding (STE, isotropic B-tensor), and  $\beta = -\frac{1}{2}$  for planar tensor encoding (PTE, two equal nonzero eigenvalues) [15–20].

Imaging voxels in the brain have vastly different fiber orientation dispersion and, as a result, distinct orientations and degrees of anisotropy of the underlying  $\mathcal{P}(D)$ . It is therefore natural for a dMRI measurement to probe all directions uniformly. The most general B-tensor is defined by its shape (3 eigenvalues summing up to the diffusion weighting  $b$ ), and the 3 orientational dof. Uniformly sampling all the orientations of B amounts to acting on it by all possible elements of the SO(3) group. Thus, a fixed- $b$  “shell” for a generic B-tensor is the group manifold of SO(3), which is the 3-dimensional sphere  $\mathbb{S}^3$  (the group manifold of its universal cover SU(2)) with the antipodal points identified [47]. In other words, a fixed- $b$  shell is a quotient space  $\mathbb{S}^3/\mathbb{Z}_2$ , where the factorization modulo group  $\mathbb{Z}_2 = \{1, -1\}$  corresponds to gluing the antipodal points. Maximally isotropic coverage with B-tensors amounts to a maximally uniform sampling of such a 3-sphere.

Acquisitions with axially symmetric B-tensors (9) are invariant under SO(2) rotations around  $\hat{\mathbf{g}}$ . Factorization of the group manifold over SO(2)  $\cong \mathbb{S}^1$  (a unit circle) results in a familiar 2-dimensional spherical shell  $\mathbb{S}^2 \cong \text{SO}(3)/\text{SO}(2)$ , which can be viewed as a quotient space  $\mathbb{S}^2 \cong \mathbb{S}^3/\mathbb{S}^1$  of a 3-sphere over a circle [50]. (As  $\mathbb{Z}_2$  is a subgroup of SO(2), the factorization over it is contained in the quotient.)

Hence, the signal (1) for axially symmetric B-tensors (9), as function of the unit  $\hat{\mathbf{g}} \in \mathbb{S}^2$ , can be represented in the canonical SH basis on  $\mathbb{S}^2$ . The SH components of its logarithm  $\mathcal{L} = \ln\langle S \rangle$  up to  $O(b^2)$  can be found by averaging the compartment signal  $S = \exp[-bD^{00} - \beta b \sum D^{2m} Y^{2m}(\hat{\mathbf{g}})]$  over  $\mathcal{P}(D)$ :

$$\mathcal{L}^{00}(b, \beta) = -bD^{00} + \frac{1}{2} b^2 \left( Q^{00} + \beta^2 T^{00} \right), \quad (10a)$$

$$\mathcal{L}^{2m}(b, \beta) = -b \beta D^{2m} + \frac{1}{2} b^2 \left( \beta Q^{2m} + \beta^2 T^{2m} \right), \quad (10b)$$

$$\mathcal{L}^{4m}(b, \beta) = \frac{1}{2} b^2 \beta^2 T^{4m}. \quad (10c)$$

While components of D and Q appear naturally using Eqs. (3) and (8a), the components (8b) of T arise via the triple SH integration (S8). The corollaries of Eqs. (10) are as follows:

- (i) *Sufficiency*: Axially symmetric family (9) on the quotient space  $\mathbb{S}^2$  is sufficient for estimating all 21 dof of C; the entire SO(3) manifold (non-axial B) is not necessary.
- (ii) *Necessity*: To estimate all tensor components, one needs 3 distinct combinations  $(b, \beta)$ , with at least 2 nonzero  $b$  and at least 2 nonzero  $\beta$  (i.e., 2 non-STE B tensors).
- (iii) *STE* ( $\beta = 0$ ) can be used to isolate  $Q^{00}$ , as  $\mathcal{L}_{STE} = -bD^{00} + \frac{1}{2} b^2 Q^{00}$  up to  $O(b^2)$  [12, 19, 20, 51].
- (iv) *Conventional LTE* ( $\beta = 1$ ) alone cannot disentangle  $Q^{(\ell)}$  and  $T^{(\ell)}$ , for both  $\ell = 0$  and 2, from their sums.

As LTE plays a major role in everyday dMRI and in publicly available datasets [34–38], we now consider it in detail.

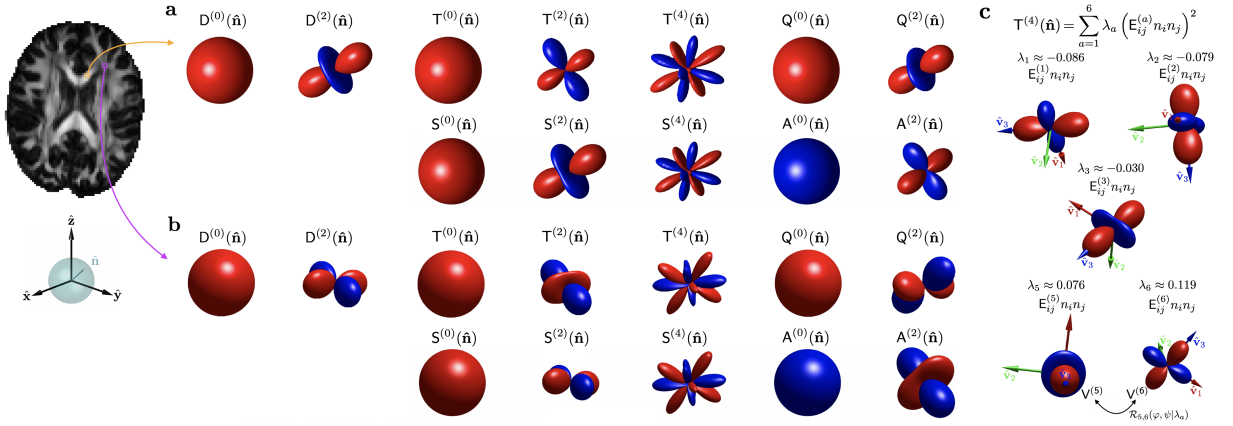


FIG. 2. Irreducible decompositions of D and C tensors, Eqs. (4), (7), and (16), for two white matter voxels: (a) corpus callosum — highly aligned fibers, and (b) longitudinal superior fasciculus — crossing fibers. Glyphs are color-coded by the sign (red = positive) while the radius represents the absolute value (rescaled to similar sizes). (c) Representation of the eigentensor decomposition, Eq. (59) in *Materials and Methods*, of  $T^{(4)}$  for the crossing fiber voxel shown in (b). The 6 invariants of  $T^{(4)} = S^{(4)}$  (cf. Fig. 3) correspond to 4 dof from  $\lambda_a$  (here  $\lambda_4 = 0$ ,  $E_{ij}^{(4)} \propto \delta_{ij}$ , and  $\sum_{a=1}^6 \lambda_a = 0$ ), and 2 dof defining the relative orientations among any pair of eigentensors  $E_{ij}^{(a)}$ .

### LTE versus other B shapes: SA decomposition

For LTE,  $B_{ij}B_{kl} \rightarrow b^2 g_i g_j g_k g_l$  becomes symmetric in all indices, and Eq. (1) turns into the diffusion kurtosis imaging (DKI) signal representation [52]:

$$\ln \langle S \rangle = -bD(\hat{\mathbf{g}}) + \frac{b^2}{2} S(\hat{\mathbf{g}}) + O(b^3), \quad S(\hat{\mathbf{g}}) = S_{ijkl} g_i g_j g_k g_l, \quad (11)$$

where  $S$ , the *fully symmetric* part of  $C$ ,

$$S_{ijkl} = C_{(ijkl)} = \frac{1}{3}(C_{ijkl} + C_{iljk} + C_{ikjl}) \equiv \frac{1}{3}D_0^2 W_{ijkl}, \quad (12)$$

is proportional to the dimensionless *kurtosis tensor*  $W$  — a 3d generalization of the kurtosis excess for the probability distribution of molecular displacements [52]. The notation [45] for symmetrization over tensor indices between (...) is assumed henceforth. Since  $W$  and  $S$  contain the same information, we will focus on  $S$ , and refer to both  $S$  and  $W$  as kurtosis.

Kurtosis splits into irreducible components with  $\ell = 0, 2, 4$ :

$$S_{ijkl} = S^{00} \delta_{(ij} \delta_{kl)} + \sum_{m=-2}^2 S^{2m} \mathcal{Y}_{(ij}^{2m} \delta_{kl)} + \sum_{m=-4}^4 S^{4m} \mathcal{Y}_{ijkl}^{4m} \quad (13)$$

such that  $S(\hat{\mathbf{g}}) = S^{(0)} + S^{(2)}(\hat{\mathbf{g}}) + S^{(4)}(\hat{\mathbf{g}})$ , where spherical tensors  $S^{(0)}$ ,  $S^{(2)}$  and  $S^{(4)}$  are parametrized by  $2\ell + 1 = 1, 5$  and  $9$  SH coefficients, respectively, totaling  $1 + 5 + 9 = 15$  dof, found from  $S_{ijkl}$  via Eqs. (50) in *Materials and Methods*.

The remaining  $21 - 15 = 6$  dof of  $C$  are contained in the *asymmetric* (not antisymmetric!) part  $A$  of  $C$ :

$$A_{ijkl} = C_{ijkl} - C_{(ijkl)} = \frac{1}{3}(2C_{ijkl} - C_{iljk} - C_{ikjl}). \quad (14)$$

To measure all dof of  $C$ , and thereby to access  $A$ , the necessary and sufficient condition is the corollary (ii) after Eq. (10), which makes the requirement rank  $B > 1$  [19] more precise.

Although  $A$  is a 4th-order Cartesian tensor, it has only 6 dof, and thus it is equivalent to a symmetric  $3 \times 3$  tensor [53, 54]:

$$A_{pq} = \epsilon_{ikp} \epsilon_{jlq} A_{ijkl} \quad (15a)$$

$$= \delta_{pq} (A_{iikk} - A_{ikik}) + 2(A_{pkqk} - A_{pqkk}), \quad (15b)$$

$$A_{ijkl} = \frac{1}{6}(\epsilon_{ikp} \epsilon_{jlq} + \epsilon_{ilp} \epsilon_{jkq}) A_{pq}, \quad (15c)$$

where  $\epsilon_{ijk}$  is the fully antisymmetric Levi-Civita tensor. Thus, analogously to Eq. (4), tensor  $A$  splits into the irreducible components with  $\ell = 0$  and  $2$ , cf. Eqs. (50).

To sum up, we obtained the *SA decomposition* of  $C$  tensor

$$C = S \oplus A, \quad S = S^{(0)} \oplus S^{(2)} \oplus S^{(4)}, \quad A = A^{(0)} \oplus A^{(2)}, \quad (16)$$

where the dof count holds:  $21_C = (1 + 5 + 9)_S + (1 + 5)_A$ . The separation of information accessible through LTE ( $S$ ) vs beyond-LTE ( $A$ ) implies that the SA decomposition is *LTE-driven*. Hundreds of thousands datasets acquired with LTE and moderate diffusion weightings are available [34–38], and thus are sensitive to the information present in  $S$  only.

The contributions of SA decomposition to  $O(b^2)$  term of the cumulant expansion (1) for  $B$  tensor family (9) are

$$B_{ij}B_{kl}S_{ijkl} = b^2 \left[ \frac{5+4\beta^2}{9} S^{(0)} + \frac{7\beta+2\beta^2}{9} S^{(2)}(\hat{\mathbf{g}}) + \beta^2 S^{(4)}(\hat{\mathbf{g}}) \right], \quad (17a)$$

$$B_{ij}B_{kl}A_{ijkl} = \frac{2}{9}b^2 \left[ (1 - \beta^2)A^{(0)} - \beta(1 - \beta)A^{(2)}(\hat{\mathbf{g}}) \right]. \quad (17b)$$

To obtain Eqs. (17), we used Eq. (15) and Supplementary Eq. (S1), such that  $S^{(0)} \equiv S^{00}$ ,  $A^{(0)} \equiv A^{00} = \frac{1}{3}A_{ppp} = \frac{1}{3}(A_{iikk} - A_{ikik})$ , and  $A^{(2)}(\hat{\mathbf{g}}) = A_{pq}^{(2)} g_p g_q$ . As expected, STE is sensitive only to the isotropic parts  $S^{(0)}$  and  $A^{(0)}$ , while LTE couples to  $S(\hat{\mathbf{g}})$  and is insensitive to  $A(\hat{\mathbf{g}})$  (Eq. (17b) vanishes). PTE couples to the  $A$  tensor ellipsoid, Eq. (17b) yielding  $+b^2/6 A(\hat{\mathbf{g}})$ , and to the combination  $b^2(\frac{2}{3}S^{(0)} - \frac{1}{3}S^{(2)}(\hat{\mathbf{g}}) +$

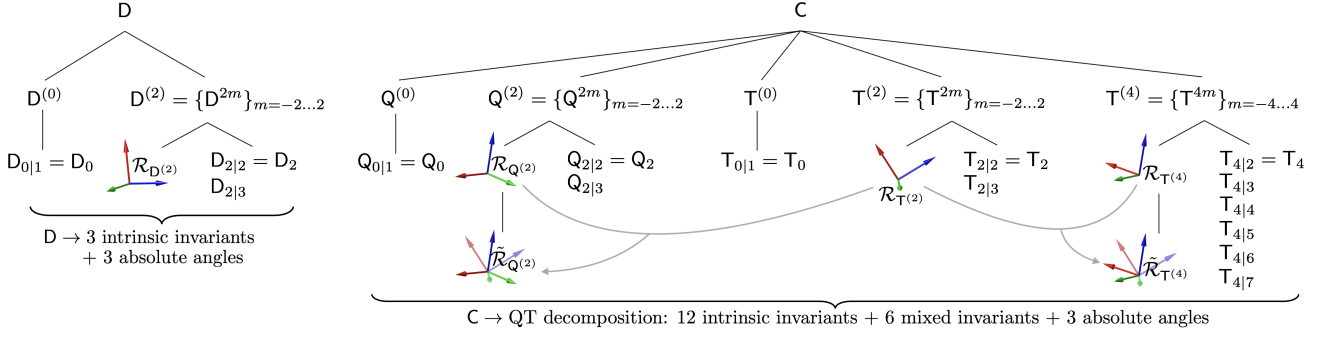


FIG. 3. Irreducible decompositions of tensors  $D$  and  $C$  (into  $Q$  and  $T$ ), Eqs. (4)–(6). Each irreducible component has its intrinsic invariants (1 for  $\ell = 0$ ; 2 for  $\ell = 2$ ; and 6 for  $\ell = 4$ ). Together with these  $1 + 2 + 1 + 2 + 6 = 12$  intrinsic invariants,  $C$  has  $3 \cdot 3 = 9$  basis-dependent absolute angles defining the orientations of its  $T^{(2)}$ ,  $T^{(4)}$ , and  $Q^{(2)}$  via the rotation matrices  $\mathcal{R}_{Q^{(2)}}$ ,  $\mathcal{R}_{T^{(2)}}$ , and  $\mathcal{R}_{T^{(4)}}$ , such that total dof count of  $C$  is  $21 = 12 + 9$ . Out of these 9 absolute angles, 6 dof are mixed invariants since they correspond to relative angles between  $Q^{(2)}$ ,  $T^{(2)}$  and  $T^{(4)}$ . As an example, we take  $\mathcal{R}_{T^{(2)}}$  as a reference, and compute the relative rotations  $\tilde{\mathcal{R}}_{T^{(4)}}$  and  $\tilde{\mathcal{R}}_{Q^{(2)}}$ . Maps of these invariants are shown in Fig. 4.

$\frac{1}{4}\mathbf{S}^{(4)}(\hat{\mathbf{g}})$  via Eq. (17a). At fixed  $b$ , LTE maximizes the sensitivity to  $\mathbf{S}^{(0)}$ ,  $\mathbf{S}^{(2)}$ ,  $\mathbf{S}^{(4)}$ ; STE — to  $\mathbf{A}^{(0)}$ ; and PTE — to  $\mathbf{A}^{(2)}$ .

Comparing  $\mathcal{O}(b^2)$  terms of Eqs. (10) to the half-sum of Eqs. (17), we relate the irreducible components of QT and SA decompositions:

$$\mathbf{Q}^{(0)} = \frac{5}{9}\mathbf{S}^{(0)} + \frac{2}{9}\mathbf{A}^{(0)}, \quad (18a)$$

$$\mathbf{Q}^{(2)} = \frac{7}{9}\mathbf{S}^{(2)} - \frac{2}{9}\mathbf{A}^{(2)}, \quad (18b)$$

$$\mathbf{T}^{(0)} = \frac{4}{9}\mathbf{S}^{(0)} - \frac{2}{9}\mathbf{A}^{(0)}, \quad (18c)$$

$$\mathbf{T}^{(2)} = \frac{2}{9}\mathbf{S}^{(2)} + \frac{2}{9}\mathbf{A}^{(2)}, \quad (18d)$$

$$\mathbf{T}^{(4)} = \mathbf{S}^{(4)}. \quad (18e)$$

These relations respect

$$\mathbf{S}^{(\ell)} = \mathbf{Q}^{(\ell)} + \mathbf{T}^{(\ell)}, \quad (19)$$

evident by comparing Eqs. (11) and (10) for  $\beta = 1$ , and formally setting  $\mathbf{Q}^{(4)} \equiv 0$ . Upon  $\text{SO}(3)$  rotations, components  $\mathbf{S}^{(\ell)}$ ,  $\mathbf{A}^{(\ell)}$ , or  $\mathbf{T}^{(\ell)}$ ,  $\mathbf{Q}^{(\ell)}$ , do not mix with each other.

Which decomposition is more “fundamental”? Since each representation with  $\ell = 0$  and  $\ell = 2$  enters Eq. (6) twice, any decomposition of  $C$  with two independent linear combinations of representations with  $\ell = 0$ , and separately for  $\ell = 2$ , is legitimate. The decompositions (7) and (16) are selected by their distinct physical meaning: The SA decomposition breaks symmetry between the LTE and non-LTE acquisitions, while the QT decomposition is natural to describe tissue properties.

The geometric meaning of the irreducible decompositions such as (4), (7), and (16), comes from the correspondence between spherical tensors and spherical harmonics (cf. Eq. (40) in *Materials and Methods*), Fig. 2. The  $\ell = 0$  parts give directional averages; the  $\ell = 2$  parts are responsible for glyphs parametrized by five  $Y^{2m}(\hat{\mathbf{n}})$ , turning the corresponding ball into an ellipsoid, such as  $D(\hat{\mathbf{n}}) = D_{ijn_jn_j}$  in DTI [2]. The  $\ell = 0$  and  $\ell = 2$  parts can capture a single fiber tract (a single pair of opposite lobes on a sphere, both at the  $\mathcal{O}(b)$  and  $\mathcal{O}(b^2)$  level), but cannot represent geometries with multiple pairs of lobes, such as in fiber crossings. The unique  $\mathbf{T}^{(4)} = \mathbf{S}^{(4)}$

part, parametrized by nine  $Y^{4m}(\hat{\mathbf{n}})$ , is the only part of  $C$  that captures multiple pairs of lobes coming from fiber crossings, see, e.g., Fig. 2c. Thereby, the beyond-LTE  $A$ -tensor part of  $C$  can only accommodate an ellipsoidal glyph shape — albeit physically distinct from that of the diffusion tensor.

As for the parameter estimation, one can either directly use Eqs. (10), or go the SA route (12) and (14) to compute the irreducible components  $\mathbf{S}^{(\ell)}$  and  $\mathbf{A}^{(\ell)}$  [Eqs. (50) in *Materials and Methods*], and then transform to QT via Eqs. (18). Once the irreducible components of  $Q$  and  $T$  tensors are known, tissue properties (compartmental spherical tensor covariances) can be found by inverting Eqs. (8), see Supplementary Eqs. (S16).

### Invariants: intrinsic and mixed

Tensor invariants are the combinations of parameters that do not change upon rotations of the basis. We now construct all invariants of  $C$  within either QT or SA decomposition, by splitting them into the ones intrinsic to a given irreducible representation, and the ones mixing representations. Let us define *intrinsic invariants* as those that belong purely to a single irreducible component, such as  $\mathbf{Q}^{(\ell)}$  and  $\mathbf{T}^{(\ell)}$  in Eq. (7), or  $\mathbf{S}^{(\ell)}$  and  $\mathbf{A}^{(\ell)}$  in Eq. (16). Conversely, *mixed invariants* determine the relative orientations between different irreducible components with  $\ell > 0$ , such as between  $\mathbf{T}^{(2)}$  and  $\mathbf{T}^{(4)}$ . In what follows, we will focus on the invariants of the QT decomposition, Fig. 3, with all maps for a human brain shown in Fig. 4. A completely analogous treatment yields the corresponding  $\mathbf{S}$  and  $\mathbf{A}$  invariants, cf. Supplementary Fig. S1.

How many intrinsic and mixed invariants are there? First note that the total number of invariants for any tensor equals its number of dof minus 3 angles defining its overall orientation [55], yielding 3 for  $D$  (DTI), 12 for  $\mathbf{S}$  or  $\mathbf{W}$  (DKI), and 18 for  $C$ . Applying this argument to each irreducible representation, the number of intrinsic invariants is 1 for  $\ell = 0$ , and  $(2\ell + 1) - 3 = 2(\ell - 1) = 2, 6, \dots$  for  $\ell = 2, 4, \dots$ . This yields  $(1 + 2 + 6) + (1 + 2) = 12$  intrinsic invariants of  $C$ , Fig. 3.

The isotropic,  $\ell = 0$  component of a symmetric tensor is an

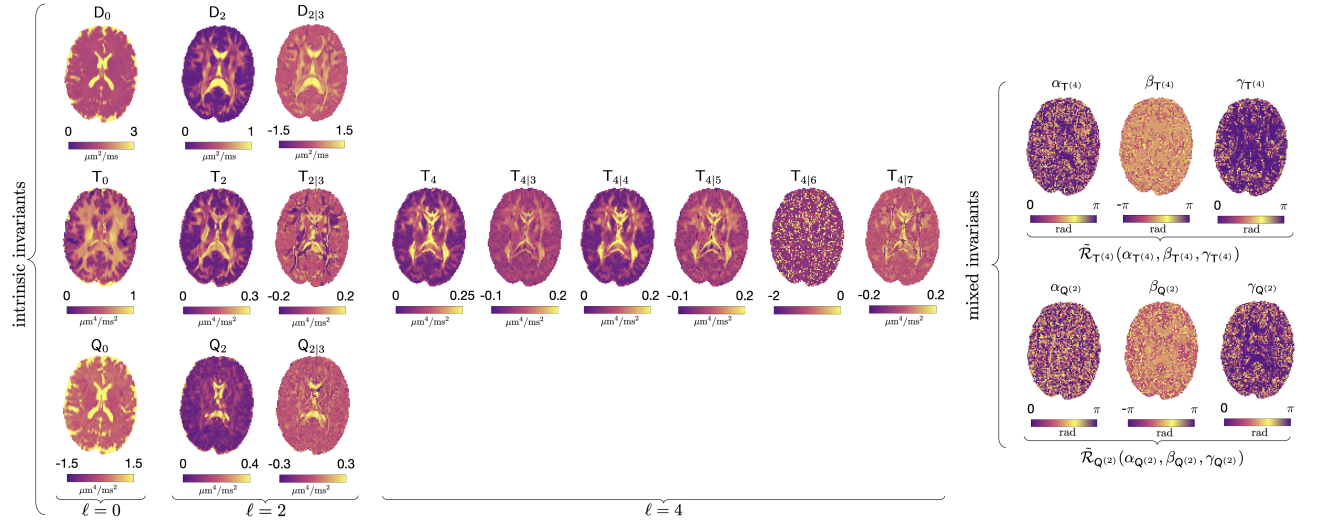


FIG. 4. RICE maps for a normal brain (33 y.o. male). Intrinsic invariants for each irreducible decomposition of  $D$ ,  $T$  and  $Q$  are shown as powers of corresponding traces, to match units of  $D$  and  $C$ . The 6 mixed invariants correspond to Euler angles of eigenframes of  $T^{(4)}$  and  $Q^{(2)}$  relative to that of  $T^{(2)}$  (see text). The underlying tissue microstructure introduces correlations between invariants: e.g. small relative angles  $\tilde{\beta}$  in white matter tracts exemplify the alignment of eigenframes of different representations of  $SO(3)$  with the tract.

invariant, normalized here to its angular average as in Eq. (5):

$$\begin{aligned} A_0 &\equiv A^{00} = \overline{A(\hat{\mathbf{n}})} = \frac{1}{3} A_{ii}, \\ S_0 &\equiv S^{00} = \overline{S(\hat{\mathbf{n}})} = \frac{1}{3} S_{iijj}, \end{aligned} \quad (20)$$

cf. Eq. (50). The respective invariants  $Q_0 \equiv Q^{00}$  and  $T_0 \equiv T^{00}$  are given in terms of  $S_0$  and  $A_0$  via Eqs. (18a) and (18c).

Consider now the irreducible components with  $\ell = 2$ . We take  $D^{(2)}$  as an example, with the analogous definitions for  $T^{(2)}$ ,  $Q^{(2)}$ ,  $S^{(2)}$ , and  $A^{(2)}$ . Among the 5 dof, 3 angles define the orientation of the glyph  $D^{(2)}(\hat{\mathbf{n}})$  and are not invariants. The remaining 2 dof parametrize the 3 eigenvalues that sum up to zero trace. The corresponding 2 invariants can be written as traces of the powers of  $D^{(2)}$ , where we introduce the index notation  $\ell|n$  useful for higher  $\ell$  in what follows:

$$D_{2|n} = \left( \frac{2}{3} \text{tr} (D^{(2)})^n \right)^{1/n}, \quad n = 2, 3. \quad (21)$$

Since the  $n = 2$  ( $L_2$ -norm) invariants play special role, we will henceforth drop the  $n = 2$  index for all degrees  $\ell \geq 2$ , Fig. 3.

Based on the definition (21), the square of  $D_2 \equiv D_{2|2}$ ,

$$D_2^2 = 2 \mathbb{V}_\lambda(D), \quad \mathbb{V}_\lambda(D) \equiv \frac{1}{3} \sum_{i=1}^3 (\lambda_i - \bar{D})^2, \quad (22)$$

is related to the variance  $\mathbb{V}_\lambda(D)$  of the eigenvalues of  $D$ . Geometrically,  $D_2^2$  characterizes the *directional variance*

$$\text{var} D(\hat{\mathbf{n}}) = \overline{D^2(\hat{\mathbf{n}})} - D_0^2 = \frac{1}{3} D_2^2, \quad D_2^2 \equiv \sum_m D^{2m*} D^{2m}, \quad (23)$$

cf. the expansion (3) and SH orthogonality. The equivalence of the directional and eigenvalue variances [31] is readily seen in the eigenbasis: for  $D^{(2)} = \text{diag} \{ \eta_1, \eta_2, -\eta_+ \}$ , where  $\eta_\pm =$

$\eta_1 \pm \eta_2$ , using  $D^{2m} = \frac{2}{3} \mathcal{Y}_{ij}^{2m*} D_{ij}$ , cf. Eq. (50) from *Materials and Methods*, we get  $D^{2,\pm 2} = \eta_- / \sqrt{6}$ ,  $D^{2,\pm 1} = 0$ , and  $D^{20} = -\eta_+$ , proving  $\sum_m |D^{2m}|^2 = 2 \cdot \frac{1}{3} (\eta_1^2 + \eta_2^2 + \eta_+^2)$ , cf. Eq. (22).

The invariants  $D_0$ ,  $D_2$ , and  $D_{2|3}^3 \propto \det D$  (the volume of the ellipsoid  $D(\hat{\mathbf{n}})$ ), provide 3 symmetrized combinations of the eigenvalues of  $D^{(0)} \oplus D^{(2)}$  which fully determine its shape.

For the  $\ell = 4$  components  $T^{(4)} = S^{(4)}$ , the picture is more complex. The 3 angles determine the orientation of the glyph  $T^{(4)}(\hat{\mathbf{n}}) = \sum_{m=-4}^4 T^{4m} Y^{4m}(\hat{\mathbf{n}})$ , while the remaining 6 dof determine its shape (Fig. 2a,b). Here we construct the principal invariant  $T_4 \equiv T_{4|2}$ , the glyph variance analogously to Eq. (23):

$$\text{var} T^{(4)}(\hat{\mathbf{n}}) = \frac{1}{9} T_4^2, \quad T_4^2 \equiv \sum_m T^{4m*} T^{4m} = \frac{8}{35} T_{ijkl}^{(4)} T_{ijkl}^{(4)}, \quad (24)$$

where the normalization factor in the last equality follows from Eq. (43). The remaining 5 intrinsic invariants are constructed in Eq. (63) of *Materials and Methods*.

The relative angles between irreducible components of a given tensor do not change upon rotations (the tensor transforms as a whole). Hence,  $18 - 12 = 6$  dof define the two sets of mixed invariants of  $C$  that parametrize the relative rotations between the frames of  $T^{(4)}$ ,  $Q^{(2)}$ , and  $T^{(2)}$ . Without the loss of generality, we take them as the Euler angles that define active rotations  $\tilde{\mathcal{R}}_T^{(4)}(\alpha_T^{(4)}, \beta_T^{(4)}, \gamma_T^{(4)})$  and  $\tilde{\mathcal{R}}_Q^{(2)}(\alpha_Q^{(2)}, \beta_Q^{(2)}, \gamma_Q^{(2)})$  of the  $T^{(2)}$  frame along  $z$  by  $\alpha$ , then along new  $x'$  by  $\beta$ , and along new  $z''$  by  $\gamma$  to obtain the  $T^{(4)}$  and  $Q^{(2)}$  frames (Fig. 3). These are mapped for the human brain in the right panel of Fig. 4 (cf. Supplementary Fig. S1 for  $S$  and  $A$ ).

The major and minor symmetries of  $C$  mimic those of the elasticity tensor in continuous media. The proposed construction of tensor invariants via representation theory has the benefit of symmetry and geometric meaning, as compared to approaches within the elasticity theory [40–44], and later in

dMRI [56–58]. Previous works used a Cartesian representation of  $\mathbf{C}$  as a symmetric  $6 \times 6$  matrix (Kelvin/Voigt notation, Eq. (56) in *Materials and Methods*). The invariants (generally, not a complete set) were introduced as coefficients of the characteristic polynomial of two variables in the  $6 \times 6$  matrix representation of  $\mathbf{C}$  [42, 56] or of  $\mathbf{S}$  [57], or via Hilbert’s theorem on non-negative ternary quartics for  $\mathbf{S}$  [58].

### Previously used dMRI contrasts from RICE

The present unifying group theory approach allows us to express all previously used  $\mathcal{O}(b^2)$  dMRI contrasts, sometimes related to specific acquisition schemes, via the smallest possible subset of the full system of invariants. Below we express the most popular contrasts in terms of only 4 invariants: 2 from  $\mathbf{D}$  ( $D_0$  and  $D_2$ ), and 2 from  $\mathbf{C}$  ( $Q_0$  and  $T_0$ ).

The  $\mathcal{O}(b)$  contrasts, MD (5) and fractional anisotropy

$$\text{FA} \equiv \sqrt{\frac{3}{2} \frac{\langle \mathbb{V}_\lambda(\mathbf{D}) \rangle}{\langle \mathbb{V}_\lambda(\mathbf{D}) \rangle + D_0^2}} = \sqrt{\frac{3D_2^2}{2D_2^2 + 4D_0^2}} \quad (25)$$

[cf. Eq. (22)], involve only  $D_0$  and  $D_2$ . Although the dimensionless ratio  $D_2/D_0$  is a more natural way to quantify the anisotropy of  $\mathbf{D}$  tensor given Eq. (23), the function (25) of  $D_2/D_0$ , bounded by  $0 \leq \text{FA} \leq 1$ , has been widely used; the bounding leads to a less transparent noise propagation.

Including  $Q_0$  and  $T_0$  yields a number of  $\mathcal{O}(b^2)$  contrasts. We begin with mean kurtosis (MK), cf. Eqs. (12) and (19):

$$\text{MK} \equiv \overline{\mathbf{W}(\hat{\mathbf{n}})} = W_0 = \frac{3\overline{\mathbf{S}(\hat{\mathbf{n}})}}{D_0^2} = \frac{3S_0}{D_0^2}, \quad S_0 = Q_0 + T_0, \quad (26)$$

defined via the directional average of  $\mathbf{W}$  [59, 60]. Eq. (26) is sometimes referred to as mean kurtosis tensor (MKT) [61], as it is equivalent to the tensor trace  $W_0 = \frac{1}{5}W_{iijj}$  and, thus, can be computed fast and precisely. The original DKI paper [52] defined mean kurtosis as the directional average of  $K(\hat{\mathbf{n}}) = 3\overline{\mathbf{S}(\hat{\mathbf{n}})}/D^2(\hat{\mathbf{n}})$ . While perhaps more intuitive, that definition suffers from two drawbacks. First, it cannot be compactly represented as a trace of a tensor [akin to Eqs. (21) and (63)] due to a nontrivial directional dependence of the denominator. Indeed, as  $K(\hat{\mathbf{n}})$  involves an *infinite series* in the powers of  $\hat{\mathbf{n}}$  due to the expansion of  $1/D^2(\hat{\mathbf{n}})$  in the powers of  $D^{(2)}(\hat{\mathbf{n}})$ , it cannot be written as a convolution of a product  $n_i n_j \dots$  with a tensor or even a few tensors [62]. Second,  $\overline{K(\hat{\mathbf{n}})}$  has lower precision than Eq. (26), and is strongly affected by outliers coming from low-diffusivity directions, for which  $D(\hat{\mathbf{n}}) \ll D_0$ .

The curvature  $\mathbb{V}_1 = Q_0$  of the STE cumulant series  $\mathcal{L}_{\text{STE}}$  [item (iii) below Eqs. (10)] is known as the *isotropic variance* [19, 20]. Speaking precisely, it is the variance of isotropic components of compartment tensors. The directional average of the LTE signal, represented in the cumulant form  $\ln\langle \hat{S}_{\text{LTE}} \rangle = -bD_0 + \frac{1}{2}b^2\mathbb{V}_A + \mathcal{O}(b^3)$ , defines the so-called *anisotropic variance* [51, 63]

$$\mathbb{V}_A \equiv \left\langle \overline{D^2(\hat{\mathbf{n}})} \right\rangle - D_0^2 = \frac{2}{5} \langle \mathbb{V}_\lambda(D) \rangle = \frac{1}{5} \langle D_2^2 \rangle = T_0 + \frac{1}{5}D_2^2, \quad (27)$$

proportional to the variance (22) of the eigenvalues of compartmental  $D$  averaged over  $\mathcal{P}(D)$ . Note that taking spherical mean of LTE signal before the logarithm makes  $\mathbb{V}_A$  a moment, rather than a cumulant:  $\langle D_2^2 \rangle = \sum_m \langle D^{2m*} D^{2m} \rangle = 5T_0 + \sum_m D^{2m*} D^{2m}$ , cf. Eq. (55). The above variances define the isotropic and anisotropic kurtoses  $K_{I,A} = 3\mathbb{V}_{I,A}/D_0^2$ , cf. Eq. (26) [19, 20, 51, 63, 64]. Note that this somewhat misleading nomenclature refers to iso/anisotropic components of compartmental diffusion tensors, while all the above quantities correspond to the *fully isotropic* ( $\ell = 0$ ) parts of  $\mathbf{C}$ , Eq. (6).

Finally, the analogy with Eq. (25) has motivated the definition of *microscopic fractional anisotropy* [19, 23, 51, 63]

$$\mu\text{FA} \equiv \sqrt{\frac{3}{2} \frac{\langle \mathbb{V}_\lambda(D) \rangle}{\langle \mathbb{V}_\lambda(D) \rangle + D_0^2}} = \sqrt{\frac{15T_0 + 3D_2^2}{10T_0 + 2D_2^2 + 4D_0^2}}. \quad (28)$$

Writing  $\mu\text{FA}$  using RICE invariants enables its evaluation without the need to assume axial symmetry for  $D$  and/or a specific functional form for  $\mathcal{P}(D)$ , as in Refs. [20, 51]. Note that the definition of  $\mu\text{FA}$  is inconsistent, in a sense that the averages over  $\mathcal{P}(D)$  are taken in the numerator and denominator separately, i.e.,  $\mu\text{FA}$  is *not* the compartmental  $\text{FA}(D)$  averaged over  $\mathcal{P}(D)$  [65]. Unfortunately, information for calculating voxel-averaged  $\langle \text{FA}(D) \rangle$  is not contained in the  $\mathcal{O}(b^2)$  signal, as it involves all higher-order cumulants.

All the above 6 popular contrasts —  $W_0$ ,  $\mathbb{V}_{I,A}$ ,  $K_{I,A}$ ,  $\mu\text{FA}$ — rely just on two  $\ell = 0$  invariants of  $\mathbf{C}$ , and are thereby redundant. Contrasts involving higher-order invariants have been largely unexplored. Empirically, one can rationalize this as the invariants decrease with  $\ell$ , shown in Fig. 5a for the  $\ell = 2$  and  $\ell = 4$  principal invariants relative to their  $\ell = 0$  counterparts. For example, the 9 elements of  $\mathbf{S}^{(4)}$  are  $\sim 5 - 10$  times smaller than  $S_0$ . Such decrease with  $\ell$  is more pronounced in gray matter, and less so in crossing fibers or highly aligned white matter regions, e.g., the corpus callosum.

Invariants with  $\ell > 0$  quantify the anisotropies of the irreducible components of  $\mathbf{C}$  (while  $\mu\text{FA}$  does not characterize the anisotropy of any specific tensor). Is there a natural definition for an overall anisotropy measure of a higher-order tensor, analogous to  $D_2$  or  $\text{FA}$  for the 2nd-order tensor? Our approach suggests that each anisotropic irreducible component is characterized by its own independent invariants, such as  $S_2$  and  $S_4$  for the  $\mathbf{S}$  tensor. Combining such invariants into a single metric seems arbitrary and mixes different symmetry sources. An example is the *kurtosis fractional anisotropy* (KFA) [60, 66]:

$$\text{KFA} \equiv \frac{\|\mathbf{S} - \mathbf{S}^{(0)}\|_F}{\|\mathbf{S}\|_F} = \sqrt{\frac{14S_2^2 + 35S_4^2}{40S_0^2 + 14S_2^2 + 35S_4^2}}, \quad (29)$$

where we express the Frobenius norm  $\|\mathbf{S}\|_F^2 \equiv S_{ijkl}S_{ijkl} = \sum_\ell \zeta(4, \ell) S_\ell^2$  in terms of the principal invariants  $S_\ell$  using Eq. (48). Akin to  $\text{FA}$ ,  $\text{KFA}$  is bounded between 0 and 1. However, it seems equally reasonable to replace the Frobenius norm with the directional average  $\overline{\mathbf{S}^2(\hat{\mathbf{n}})} = \sum_\ell S_\ell^2 / (2\ell + 1)$ , yielding different relative weights with which the invariants  $S_\ell$  would enter. As there is no “best” combination of invariants with different  $\ell$ , it is generally logical to consider them separately.

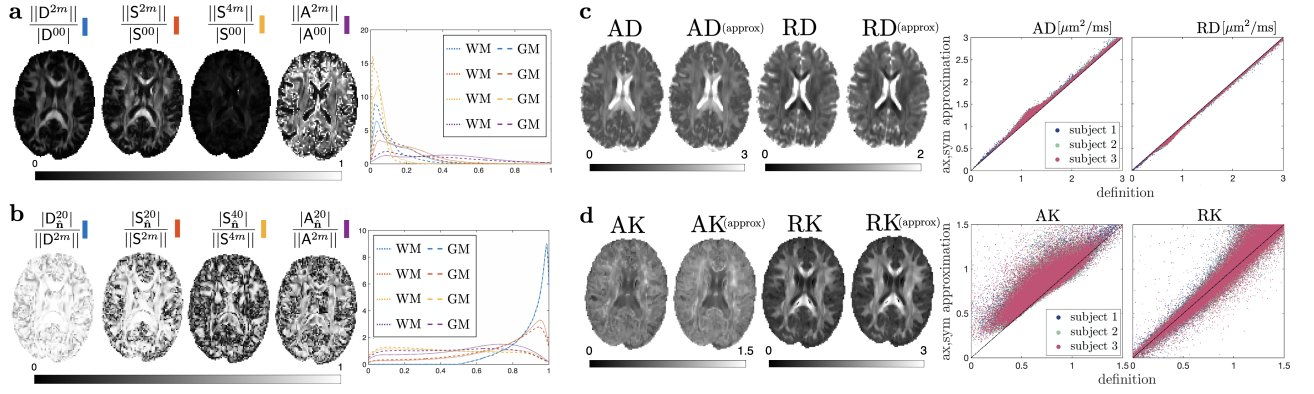


FIG. 5. Significance of  $\ell > 0$  and axial symmetry in healthy brains. (a) Normalized maps of the  $L_2$ -norms for degree- $\ell$  components of  $D$ ,  $S \propto W$ , and  $A$ , and their histograms for white and gray matter (WM, GM) voxels.  $S^{4m}$  elements are  $5 - 10\times$  smaller than  $S^{00}$ . (b) Relative contribution of the  $m = 0$  components in the principal fiber coordinate frame, such ratio = 1 for perfect axial symmetry. (c,d): Axial and radial projections of the diffusion (c) and kurtosis (d) tensors, calculated both exactly and via Eqs. (30) relying on the axial symmetry approximation.

There is a case where combining invariants with different  $\ell$  is natural. The *axial and radial kurtoses*  $W_{\parallel}$  and  $W_{\perp}$  [67, 68] are projections of the kurtosis tensor  $W = 3S/D_0^2$  [Eq. (12)] onto the principal fiber axis  $\hat{v}$  (the eigenvector for the largest eigenvalue of  $D$ ), and transverse to it. In general, they are not rotational invariants, as  $W \propto S$  does not “know” about  $D$  and its eigenvectors. However, in voxels with a dominant fiber direction  $\hat{v}$ , microstructure aligns the  $S$  and  $D$  tensors, Fig. 4, and axial/radial nomenclature becomes meaningful. Under an extra assumption of *axial symmetry* of  $S$  around  $\hat{v}$ , we express its projections via the principal invariants for  $\ell = 0, 2, 4$ :

$$D_{\parallel}^{\text{ax,sym}} = D_0 + D_2, \quad (30a)$$

$$D_{\perp}^{\text{ax,sym}} = D_0 - \frac{1}{2}D_2, \quad (30b)$$

$$W_{\parallel}^{\text{ax,sym}} = \frac{3}{D_0^2} (S_0 + S_2 + S_4), \quad (30c)$$

$$W_{\perp}^{\text{ax,sym}} = \frac{3}{D_0^2} \left( S_0 - \frac{1}{2}S_2 + \frac{3}{8}S_4 \right), \quad (30d)$$

without the need to transform to the eigenbasis of  $D$ . Indeed, in the basis with  $z$ -axis along  $\hat{v}$ , only  $m = 0$  components are nonzero for each  $\ell$ . This implies that  $D_{\ell} = |D^{\ell 0}|$  and  $S_{\ell} = |S^{\ell 0}|$ . In this basis,  $Y^{\ell 0}(\hat{z}) = 1$  for  $\parallel$  invariants; the average of  $Y^{\ell 0}(\hat{n}) = P_{\ell}(\hat{n} \cdot \hat{z})$  around the equator for  $\perp$  invariants is given by Legendre polynomial values  $P_2(0) = -\frac{1}{2}$  and  $P_4(0) = \frac{3}{8}$ .

How valid is the axial symmetry assumption? In Fig. 5b, we rotate all voxels’ principal fiber axes  $\hat{n}$  to  $\hat{z}$ , and quantify the axial symmetry in each irreducible component  $F^{(\ell)}$  via the ratios  $|F_{\hat{n}}^{\ell 0}|/F_{\ell}$  of the  $m = 0$  component to its principal invariant, the 2-norm  $F_{\ell} = \|F^{\ell m}\|$  over all  $m$ . For the  $D$  tensor, the ratio  $|D_{\hat{n}}^{20}|/D_2 = (1 + \eta_-^2/3\eta_+^2)^{-1/2}$  in the notations after Eq. (23). Perfect axial symmetry would correspond to the unit ratios. Fig. 5b shows that  $D^{(2)}$  and  $S^{(2)}$  have a high axial symmetry, while the opposite holds for  $S^{(4)}$  and  $A^{(2)}$ .

Figures 5c and 5d show axial and radial projections for  $D$  and  $S$ : the exact ones calculated by projecting onto principal fiber direction  $\hat{v}$  and transverse to it, and the ones via assuming axial symmetry, Eqs. (30). Although  $S^{(4)}$  is generally not axially symmetric, a good agreement between exact and approximate

expressions is found in the whole brain because  $S^{(4)}$  are much smaller than  $S^{(0)}$  and  $S^{(2)}$ .

### New invariants

The QT decomposition is motivated by the separation of different sources of covariances of compartmental diffusivities. While the  $\ell = 0$  parts of  $T$  and  $Q$  have been studied in the dMRI literature under different names, their anisotropic complements have remained unexplored. They provide access to novel rotationally invariant tissue contrasts.

Overall, just 6 independent invariants:  $D_0$  and  $D_2$ ;  $S_0$  and  $A_0$  (equivalently,  $Q_0$  and  $T_0$ ); and  $S_2$  and  $S_4$ , are enough to synthesize all previously used model-independent dMRI contrasts up to  $O(b^2)$ . Since individual DTI eigenvalues may be used as contrasts, the total number of previously studied  $O(b^2)$  invariants (explicitly or implicitly) is at most 3 from  $D$  ( $D_0, D_2, D_{2|3}$ ), and at most 4 from  $C$  ( $A_0, S_0, S_2, S_4$ ).

The remaining 14 invariants of the  $C$  tensor contain essentially unexplored information. Their definition, symmetries, and geometric meaning constitute the main results of the present comprehensive group theory-based approach. Just as an example, one can think of a novel physically motivated contrast — the size-shape correlation coefficient

$$\text{SSC} \equiv \frac{\| \langle \langle D^{00} D^{2m} \rangle \rangle \|}{\sqrt{\langle \langle (D^{00})^2 \rangle \rangle \cdot \sum_m \langle \langle D^{2m} D^{2m*} \rangle \rangle}} = \frac{1}{2} \frac{Q_2}{\sqrt{5} Q_0 T_0} \quad (31)$$

that involves  $Q_2$  and is normalized between 0 and 1, where  $\text{SSC}=0$  for independent shapes and sizes and  $\text{SSC}=1$  for a linear relationship. The  $\ell = 2$  and  $\ell = 4$  sectors of  $T$  have not been looked upon at all. The six mixed invariants relate to the underlying fiber tract geometry, quantifying correlations between eigenframes of different irreducible components. In particular, small relative angles  $\tilde{\beta}$  in Fig. 4 within major white matter tracts are set by the underlying aligned fiber geometry.

The relevance of these and other remaining RICE will be elucidated in future studies. Such a large set of complementary

TABLE I. Theoretically minimal protocols contain the minimum unique number of directions and distinct  $b$ -values (specific  $b$ -values can be altered). For STE, more than 1 direction implies rotation of the waveform for accuracy. All protocols include a  $b = 0$  image to estimate  $S|_{b=0}$ .

Fast protocols comparison, $b$ -values are in $\text{ms}/\mu\text{m}^2$		
Output maps	MD+MK	MD+FA+MK
Theoretical minimum	$6 \times \text{LTE}_{b=2}$ $1 \times \text{STE}_{b=1}$	$6 \times \text{LTE}_{b=1}$ ; $6 \times \text{LTE}_{b=2}$
 iRICE (MD+FA+MK)		$6 \times \text{LTE}_{b=1}$ ; $6 \times \text{LTE}_{b=2}$
Ref. [60]	$3 \times \text{LTE}_{b=1}$ ; $9 \times \text{LTE}_{b=2}$	
Output maps	MD+MK+ $\mu$ FA	MD+FA+MK+ $\mu$ FA
Theoretical minimum	$6 \times \text{LTE}_{b=2}$ $1 \times \text{STE}_{b=1}$ ; $1 \times \text{STE}_{b=1.5}$	$6 \times \text{LTE}_{b=1}$ ; $6 \times \text{LTE}_{b=2}$ $1 \times \text{STE}_{b=1.5}$
 iRICE (MD+FA+MK+ $\mu$ FA)		$6 \times \text{LTE}_{b=1}$ ; $6 \times \text{LTE}_{b=2}$ $3 \times \text{STE}_{b=1.5}$
Ref. [69]	$3 \times \text{LTE}_{b=0.1}$ ; $3 \times \text{LTE}_{b=0.7}$ ; $6 \times \text{LTE}_{b=1.4}$ ; $6 \times \text{LTE}_{b=2}$ $6 \times \text{STE}_{b=0.1}$ ; $6 \times \text{STE}_{b=0.7}$ ; $10 \times \text{STE}_{b=1.4}$ ; $16 \times \text{STE}_{b=2}$	

tissue contrasts is well suited for machine learning algorithms to study human development, aging and disease. Much like RGB pictures contain  $N=3$  colors,  $N=21$  invariant contrasts can be viewed as a large- $N$  generalization of computer vision data, prompting the development of large- $N$  classifiers.

For invariants not involving the  $\mathbf{A}$  tensor, one can explore hundreds of thousands human data sets from imaging consortia such as the Alzheimer’s Disease Neuroimaging Initiative (ADNI) [34], Human Connectome Project [35], UK Biobank [37], Adolescent Brain Cognitive Development (ABCD) [38], and Cambridge Centre for Ageing and Neuroscience data repository [39], which are all compatible with the DKI representation (11). A comprehensive  $\mathbf{B}$ -tensor encoding human dataset has been recently made public [70], from which all SA and QT invariants can be determined and studied.

### Minimal protocols: iRICE

Clinical dMRI is constrained by scan time. A compromise could be to use a small number of measurements (much fewer than  $1 + 6 + 21$ ) to estimate just a few  $\ell = 0$  invariants, given that they are most pronounced, Fig. 5a. The orthogonality of the STF/SH basis ensures an unbiased estimation of any sector  $\ell$  of spherical tensor components without having to estimate the entire set. Furthermore, arranging  $\mathbf{B}$ -tensors into *spherical designs* provides the minimum number of directions that guarantee such orthogonality. These ideas result in the minimal iRICE (“instant RICE”) protocols, as described below.

We first note that since the axially symmetric family (9) couples to all components of  $\mathbf{C}$ , without the loss of generality we can consider spherical designs on  $\mathbb{S}^2$  rather than on the  $\text{SO}(3)$  manifold  $\mathbb{S}^3/\mathbb{Z}_2$  of generic  $\mathbf{B}$ -tensors. Next, we remind that a spherical  $L$ -design on  $\mathbb{S}^2$  is a set of  $N_L$  points  $\{\hat{\mathbf{g}}^\alpha \in \mathbb{S}^2\}_{\alpha=1}^{N_L}$  on a unit sphere, that satisfies [71]

$$\frac{1}{N_L} \sum_{\alpha=1}^{N_L} f^{(L)}(\hat{\mathbf{g}}^\alpha) \equiv \int_{\mathbb{S}^2} f^{(L)}(\hat{\mathbf{g}}) \frac{d\Omega_{\hat{\mathbf{g}}}}{4\pi} = f^{00} \quad (32)$$

for any degree- $L$  function  $f^{(L)}(\hat{\mathbf{g}})$ , i.e., a function that can

be expressed by a truncated SH series up to degree  $L$ . In other words, any integration over  $\mathbb{S}^2$  is exactly represented by a finite sum (32) for any rotation of the set  $\{\hat{\mathbf{g}}^i\}$ , provided that the integrand is degree- $L$ , and yields its angular average  $f^{00}$ . In particular, taking  $f^{(L)}(\hat{\mathbf{g}}) = Y^{\ell m}(\hat{\mathbf{g}}) Y^{\ell' m'}(\hat{\mathbf{g}})$ , the orthogonality of  $Y^{\ell m}(\hat{\mathbf{g}})$  and  $Y^{\ell' m'}(\hat{\mathbf{g}})$  is ensured exactly in the finite- $N_L$  sums (32) for all  $\ell + \ell' \leq L$ . The smallest 2- and 4-designs are provided by tetrahedron and icosahedron vertices,  $N_2 = 4$  and  $N_4 = 12$ , respectively. However, for antipodal-symmetric  $f^{(L)}(\hat{\mathbf{n}}) = f^{(L)}(-\hat{\mathbf{n}})$  relevant for dMRI,  $N_2 = 3$  reduces to half of the octahedron vertices, and  $N_4 = 6$  to half of the icosahedron vertices, cf. Supplementary Section S5.

Constructing fixed- $b$  shells (9) from 4-designs  $\{\hat{\mathbf{g}}^\alpha\}$  allows us to become insensitive to  $\ell = 4$  terms in Eq. (10) and fit

$$\ln \frac{S(b, \hat{\mathbf{g}}^\alpha)}{S|_{b=0}} = -b \left( D_0 + \beta \sum_{m=-2}^2 D^{2m} Y^{2m}(\hat{\mathbf{g}}^\alpha) \right) + \frac{b^2}{2} \left( Q_0 + \beta^2 T_0 + \sum_{m=-2}^2 (\beta Q^{2m} + \beta^2 T^{2m}) Y^{2m}(\hat{\mathbf{g}}^\alpha) \right). \quad (33)$$

We kept the  $\ell = 2$  terms in Eq. (33), not just  $\ell = 0$ , because  $N_4 = 6$  directions are enough to obtain unbiased  $D^{2m}$  estimates (and hence, DTI) at no extra cost. Unfortunately, the  $O(b^2)$  estimates of  $\beta Q^{2m} + \beta^2 T^{2m}$  terms will be biased by the presence of  $T^{4m}$ , as the 4-design cannot detect these two as orthogonal.

Minimal 4-designs combined with required  $b$  and  $\beta$  contain fewer measurements than the total dof in  $\mathbf{D}$  and  $\mathbf{C}$ . Thus, Eq. (33) provides a method for the fastest unbiased estimation of  $D^{(0)}$ ,  $D^{(2)}$ ,  $T^{(0)}$ , and  $Q^{(0)}$  components, and the invariants (25)–(28). Table I shows the proposed minimal iRICE protocols for MD, FA, MK, based on measurements with 12  $\mathbf{B}$  tensors; and MD, FA, MK,  $\mu$ FA with 15  $\mathbf{B}$  tensors. These numbers are notably smaller than  $21 = 6 + 15$  or  $27 = 6 + 21$  needed to determine all dof (besides  $S|_{b=0}$ ). These protocols involve fewer measurements than was previously anticipated [60]. Previous fast protocols are shown for comparison.

Minimal and extensive acquisitions are compared in Figs. 6a,c. iRICE maps show a near-identical contrast, even in regions with large  $\mathbf{S}^{(4)}$  such as WM fiber crossings, de-

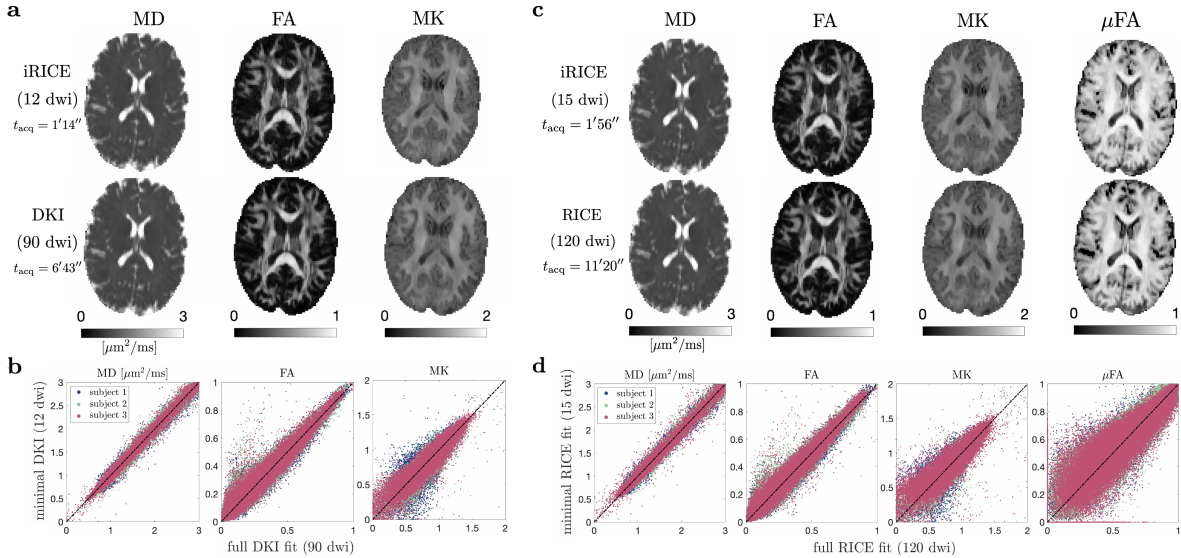


FIG. 6. Comparison of iRICE (1-2 minutes) with fully sampled acquisitions (6-11 minutes). (a,c): iRICE maps (top) vs fully sampled DKI maps (bottom) for a healthy volunteer. Panels (b) and (d) show scatter plots for all brain voxels in 3 normal volunteers (3 colors).

spite having 8-fold fewer measurements and not estimating full tensors. Scatter plots, Figs. 6b,d, do not show biases.

### Generalizations

The representation theory approach applies to any higher-order cumulant tensor. For example, the next, 6th-order cumulant at  $O(b^3)$  maps onto the addition of 3 angular momenta; the generalization of QT decomposition would yield the covariances  $\langle\langle D^{\ell m} D^{\ell' m'} D^{\ell'' m''} \rangle\rangle$ , that split into

$$\langle\langle D \otimes D \otimes D \rangle\rangle \sim \vec{6} \oplus (2 \times \vec{4}) \oplus (4 \times \vec{2}) \oplus (5 \times \vec{0}) \quad (34)$$

irreducible components, totalling 56 dof with 35 intrinsic and 18 mixed invariants. The corresponding SA decomposition yields  $\vec{6} \oplus \vec{4} \oplus \vec{2} \oplus \vec{0}$  for the fully symmetric part, and the remaining  $\vec{4} \oplus (3 \times \vec{2}) \oplus (4 \times \vec{0})$  for the asymmetric part, each with 28 dof. Probing all 56 dof of  $\langle\langle D \otimes D \otimes D \rangle\rangle$  requires non-axially symmetric B tensors [72]. In other words, this and higher-order cumulants involve waveform rotations over the  $SO(3)$  manifold  $S^3/\mathbb{Z}_2$  rather than  $S^2$ . Acquisitions sensitive to terms  $\sim b^3$  and beyond may come close or exceed the convergence radius of the cumulant expansion [73], in which case their estimation may be challenging, and a full functional form of  $\mathcal{P}(D)$  should rather be modeled. The latter has been performed using a multi-dimensional inverse Laplace transform [20, 74, 75], which requires regularization or constraints, and uses extensive, so-far clinically unfeasible acquisitions.

The present approach readily generalizes onto non-Gaussian diffusion in each tissue compartment, when compartments are characterized by their (generally, diffusion time-dependent) diffusion and kurtosis tensors  $D(t)$  and  $S(t)$ . In this case,  $C(t) = \langle\langle D(t) \otimes D(t) \rangle\rangle$  becomes the covariance tensor of the compartmental  $D(t)$ , and the additional *microscopic kurtosis*

*tensor*  $S_{\mu}(t) = \langle S(t) \rangle$  appears, given by the distribution-average of the compartmental  $S(t)$ . Separating  $C(t)$  and  $S_{\mu}(t)$  can be done via double diffusion encoding (DDE) in the limit of long mixing time [24, 64, 76]. Our methodology then allows one to represent  $C(t)$  and  $S_{\mu}(t)$  in terms of time-dependent irreducible components; for  $C(t)$ , all the above formalism applies, while  $S_{\mu}(t) = S_{\mu}^{(0)}(t) \oplus S_{\mu}^{(2)}(t) \oplus S_{\mu}^{(4)}(t)$ , Eq. (13).

### CONCLUSIONS AND OUTLOOK

Representation theory is a powerful general framework to classify symmetries and construct tensor invariants. The irreducible decompositions and their invariants apply to the diffusion and covariance tensors even beyond the Gaussian compartment framework. Based only on symmetry considerations, the formalism extends onto all 4th-order tensors with minor and major symmetries such as the elasticity tensor in continuous media [40–44], yielding applications in mechanics, geology, materials science, and soft condensed matter physics. It also generalizes onto higher-order cumulant tensors [72], mapping onto the addition of 3 or more angular momenta.

For diffusion NMR/MRI, we uncovered 14 invariants in addition to 7 previously used in the life sciences context of diagnostic MRI. Publicly available consortia dMRI datasets provide a venue to study the novel contrasts at a population level. RICE maps belong to distinct irreducible representations of rotations, and thereby represent “orthogonal” contrasts up to  $b^2$ . Such independence may improve sensitivity and specificity to detect specific tissue microstructure changes in disease, aging and development. Furthermore, the proposed minimal iRICE acquisition protocols for estimating MD, FA, MK, and  $\mu$ FA will enable clinical translation of beyond-DTI diffusion metrics hampered by long scan times.

## MATERIALS AND METHODS

### Notations

Throughout this work, sans serif font refers to voxel-wise tensors, such as  $D$ ,  $C$ ,  $A$ ,  $S$ ,  $Q$ ,  $T$ , whereas italic font refers to tensors  $D$  of the microscopic compartments. These may have either Cartesian components such as  $D_{ij}$  and  $D_{ij}$ , or spherical tensor components such as  $D^{\ell m}$  and  $D^{\ell m}$ . We refer to irreducible components, such as  $S^{(\ell)}$ , both as a collection of  $S^{\ell m}$  spherical tensor elements, or Cartesian ones  $S_{i_1 \dots i_\ell}^{(\ell)}$ . Unless specified otherwise, the order  $\ell$  of the latter will coincide with the number of Cartesian subindices since this is the most natural representation. We assume Einstein's convention of summation over repeated Cartesian subindices  $ijkl\dots$ .

Brackets  $\langle \dots \rangle$  denote averages over the compartmental diffusion tensor distribution  $\mathcal{P}(D)$ , and double brackets  $\langle\langle \dots \rangle\rangle$  denote cumulants of  $\mathcal{P}(D)$ . Finally, for readability, we omit outer parentheses when referring to tensor traces, e.g.,  $\text{tr } B = \text{tr}(B)$ ,  $\text{tr } BD = \text{tr}(BD)$ , and  $\text{tr}^\nu B = (\text{tr}(B))^\nu$ .

### Multiple Gaussian compartments

The dMRI signal from a given voxel

$$S = \langle e^{i\phi} \rangle_{\text{paths+spins}}, \quad \phi = - \int_0^t d\tau \mathbf{g}(\tau) \cdot \mathbf{r}(\tau) \quad (35)$$

is the transverse magnetization  $e^{i\phi}$  in the rotating frame, averaged over all spins traveling along all possible Brownian paths  $\mathbf{r}(\tau)$  between  $\tau = 0$  and measurement time  $t$ . Experiments are performed under the condition  $\int_0^t \mathbf{g}(\tau) d\tau = 0$  on the applied Larmor frequency gradient  $\mathbf{g}(\tau)$  [2, 5, 14]. In general, the dMRI signal is a functional of  $\mathbf{g}(t)$ , or, equivalently, of the encoding function  $\mathbf{q}(t) = \int_0^t \mathbf{g}(\tau) d\tau$ :  $S = S[\mathbf{q}(t)]$ . Even for a conventional pulsed-gradient diffusion sequence [49], one obtains a multi-dimensional phase diagram in the space of sequence parameters [7, 8].

However, after coarse-graining the dynamics within a given tissue compartment over sufficiently long  $t$ , the microstructure-induced temporal velocity correlations become forgotten, such that the distribution of spin phase  $\phi = \int_0^t d\tau \mathbf{q}(\tau) \cdot \mathbf{v}(\tau)$  becomes asymptotically Gaussian, defined by its velocity autocorrelation function  $\langle\langle v_i(\tau) v_j(\tau') \rangle\rangle \simeq 2D_{ij} \delta(\tau - \tau')$  [5, 7, 14]. The averaging in Eq. (35) over a compartment is then represented in terms of the second cumulant of the phase,  $S = e^{-B_{ij} D_{ij}}$ , and the measurement is determined by specifying the B-tensor with elements

$$B_{ij} = \int_0^t d\tau q_i(\tau) q_j(\tau) \quad (36)$$

calculated based on  $\mathbf{q}(t)$ . The distribution  $\mathcal{P}(D)$  of compartment tensors in a voxel gives rise to the overall signal [77–79]

$$S(B) = \int dD \mathcal{P}(D) e^{-\text{tr} BD} = \sum_\alpha f_\alpha e^{-\text{tr} BD^\alpha}. \quad (37)$$

Normalization  $\int dD \mathcal{P}(D) = 1$  implies  $\sum_\alpha f_\alpha = 1$ .

Equation (37) is the most general form of a signal from multiple Gaussian compartments. It is valid when the transient processes have played out, such that compartmental diffusion tensors  $D$  have all become time-independent, and thereby higher-order cumulants in each compartment are negligible [5]. In this case, the signal (37) is a function of the B-tensor:  $S[\mathbf{q}(t)] \rightarrow S(B)$ , while tissue is fully represented by the voxelwise distribution  $\mathcal{P}(D)$ . This long- $t$  picture of multiple Gaussian compartments (anisotropic and non-exchanging) underpins a large number of dMRI modeling approaches, in particular, the Standard Model (SM) of diffusion [5] and its variants [80–85]. Furthermore, this picture contains the SM extension onto different fiber populations in a voxel, lifting the key SM assumption of a single-fascicle “kernel” (response).

Given the forward model (37), an inverse problem is to restore  $\mathcal{P}(D)$  from measurements with different  $B$ . This problem is a matrix version of the inverse Laplace transform and is therefore ill-conditioned. Since in clinical settings, typical encodings are moderate ( $\text{tr} BD \sim 1$ ), the inverse problem can be formulated term-by-term for the cumulant expansion (1) of the signal (37).

### Parameter count for the cumulant series

The higher-order signal terms in Eq. (1) couple to successive cumulants of  $\mathcal{P}(D)$ . The inverse problem maps onto finding the cumulants  $\langle\langle D_{i_1 j_1} \dots D_{i_n j_n} \rangle\rangle$  (tensors of even order  $2n$ ) from a set of measurements. This becomes obvious by noting the analogy  $B \rightarrow i\lambda$  with the standard cumulant series [21]  $\ln p(\lambda) = \sum_{n=1}^{\infty} \frac{(-i\lambda)^n}{n!} \langle\langle x^n \rangle\rangle$  for the characteristic function  $p(\lambda) = \int dx e^{-i\lambda x} p(x)$  of a probability distribution  $p(x)$ , such that the  $n$ -th term in Eq. (1) is  $\frac{(-)^n}{n!} B_{i_1 j_1} \dots B_{i_n j_n} \langle\langle D_{i_1 j_1} \dots D_{i_n j_n} \rangle\rangle$ .

Hence, the introduction of the B-tensor, enabled by the Gaussian diffusion assumption, lowers the order by half: The  $2n$ -th cumulant of the phase (35) (the  $2n$ -th order term from expanding  $\ln S[\mathbf{q}(t)]$  in  $\mathbf{q}(t)$ ) maps onto the  $n$ -th cumulant  $\langle\langle D_{i_1 j_1} \dots D_{i_n j_n} \rangle\rangle$  of  $\mathcal{P}(D)$  corresponding to the  $n$ -th order of expansion of  $\ln S(B)$  in  $B$ . The number of dof for this cumulant equals to that for a fully symmetric order- $n$  tensor of dimension  $d = 6$ , which is a number of assignments of  $n$  indistinguishable objects into  $d$  distinguishable bins:  $\binom{n+d-1}{n} = (n+5)!/(n!5!) = 6, 21, 56, 126, \dots$  for  $n = 1, 2, 3, 4, \dots$ .

### Irreducible representations of SO(3)

Here we remind key aspects from representation theory of SO(3) [46, 47] used throughout this work. A  $d$ -dimensional representation of a group is a mapping of each element (rotation) onto a  $d \times d$  matrix that acts on a  $d$ -dimensional vector space. Representation theory provides a way to split a complex object (such as tensor  $D$  or  $C$ ) into a set of independent simpler ones with certain symmetries, on which a group acts. In par-

ticular, the elements of an *irreducible representation* transform among themselves, and hence can be studied separately.

Every irreducible representation of  $\text{SO}(3)$  is labeled by an integer *degree*  $\ell = 0, 1, 2, \dots$ , and acts on a  $2\ell+1$ -dimensional space of STF tensors [45] — fully symmetric and trace-free (for  $\ell > 0$ ) tensors of *order*  $\ell$  (i.e., with  $\ell$  indices). Any order- $\ell$  STF tensor (STF- $\ell$  tensor) can be represented by its  $2\ell + 1$  *spherical tensor* components  $F^{\ell m}$ ,  $m = -\ell \dots \ell$ :

$$F_{i_1 \dots i_\ell}^{(\ell)} = \sum_{m=-\ell}^{\ell} F^{\ell m} \mathcal{Y}_{i_1 \dots i_\ell}^{\ell m}, \quad (38)$$

where  $\mathcal{Y}_{i_1 \dots i_\ell}^{\ell m}$  form the standard complex-valued STF basis [45]. STF property means that a trace over any pair of indices vanishes for  $\ell \geq 2$ :  $\mathcal{Y}_{i_1 \dots i_\ell}^{\ell m} \delta_{i_n i_{n'}} \equiv 0$ ,  $1 \leq n, n' \leq \ell$ . The case  $\ell = 0$  corresponds to a (generally nonzero) scalar. For each  $\ell$ , basis STF tensors generate  $2\ell + 1$  spherical harmonics on  $\mathbb{S}^2$ :

$$Y^{\ell m}(\hat{\mathbf{n}}) = \mathcal{Y}_{i_1 \dots i_\ell}^{\ell m} n_{i_1} \dots n_{i_\ell}, \quad |\hat{\mathbf{n}}| = 1. \quad (39)$$

As a result, a spherical tensor is uniquely mapped onto a “glyph” (e.g., Fig. 2):

$$F^{(\ell)}(\hat{\mathbf{n}}) = F_{i_1 \dots i_\ell}^{(\ell)} n_{i_1} \dots n_{i_\ell} = \sum_{m=-\ell}^{\ell} F^{\ell m} Y^{\ell m}(\hat{\mathbf{n}}), \quad (40)$$

with its components  $F^{\ell m}$  being SH coefficients of the glyph.

Throughout this work, we use *Racah normalization* [86] of SH and spherical tensors (\* denotes complex conjugation):

$$\int_{\mathbb{S}^2} d\Omega_{\hat{\mathbf{n}}} Y^{\ell m*}(\hat{\mathbf{n}}) Y^{\ell' m'}(\hat{\mathbf{n}}) = \frac{4\pi}{2\ell + 1} \delta_{\ell\ell'} \delta_{mm'}. \quad (41)$$

To obtain Racah-normalized SH and basis tensors  $\mathcal{Y}_{i_1 \dots i_\ell}^{\ell m}$ , one needs to multiply the orthonormal  $Y^{\ell m}(\hat{\mathbf{n}})$  and  $\mathcal{Y}_{i_1 \dots i_\ell}^{\ell m}$  (found, e.g., in Thorne [45]) by  $\sqrt{4\pi/(2\ell + 1)}$ . Thus, Racah-normalized spherical tensor coefficients  $F^{\ell m}$  do not carry the  $\sqrt{(2\ell + 1)/4\pi}$  factors ubiquitous for the orthonormal SH. This has a benefit of the  $\ell = 0$  component being identically equal to the angular-averaged glyph since  $\mathcal{Y}^{00} \equiv 1$  (see, e.g., Eq. (5) for mean diffusivity), as well as of simplifying the relations between the SH products and Clebsch-Gordan coefficients, see Supplementary Section S2. We also use Condon-Shortley convention [87]

$$\mathcal{Y}_{i_1 \dots i_\ell}^{\ell m*} = (-1)^m \mathcal{Y}_{i_1 \dots i_\ell}^{\ell, -m}(\hat{\mathbf{n}}), \quad Y^{\ell m*}(\hat{\mathbf{n}}) = (-1)^m Y^{\ell, -m}(\hat{\mathbf{n}}), \quad (42)$$

and thus  $F^{\ell m*} = (-1)^m F^{\ell, -m}$  for real-valued  $F_{i_1 \dots i_\ell}^{(\ell)}$ .

To go from Cartesian to spherical tensor components, we invert Eq. (38) via Eq. (2.5) of Ref. [45], Eqs. (39) and (41):

$$\mathcal{Y}_{i_1 \dots i_\ell}^{\ell m*} \mathcal{Y}_{i_1 \dots i_\ell}^{\ell m'} = \frac{(2\ell - 1)!!}{\ell!} \delta_{mm'}, \quad (43)$$

where  $\ell!! \equiv \ell(\ell - 2)(\ell - 4) \dots (2 \text{ or } 1)$ , such that

$$F^{\ell m} = \frac{\ell!}{(2\ell - 1)!!} \mathcal{Y}_{i_1 \dots i_\ell}^{\ell m*} F_{i_1 \dots i_\ell}. \quad (44)$$

## Decomposition into irreducible representations

Any fully symmetric order- $L$  tensor  $F_{i_1 \dots i_L}$  (generally, with nonzero traces), such as the kurtosis tensor (13), can be decomposed into a direct sum of STF tensors  $F = F^{(L)} \oplus F^{(L-2)} \oplus \dots$  of degrees  $L, L - 2, \dots$ , (0 or 1), effectively by subtracting traces [45]. To convert this direct sum into an ordinary sum in the space of order- $L$  tensor components

$$F_{i_1 \dots i_L} = \sum_{\ell=L, L-2, \dots} F_{i_1 \dots i_L}^{(\ell)}, \quad F_{i_1 \dots i_L}^{(\ell)} = \sum_{m=-\ell}^{\ell} F^{\ell m} \mathcal{Y}_{i_1 \dots i_L}^{\ell m}, \quad (45)$$

we introduce the basis elements that are *non-STF* for  $L > \ell$ :

$$\mathcal{Y}_{i_1 \dots i_L}^{\ell m} = \mathcal{Y}_{(i_1 \dots i_\ell)}^{\ell m} \delta_{i_{\ell+1} i_{\ell+2}} \dots \delta_{i_{L-1} i_L}, \quad \ell \leq L, \quad (46)$$

through symmetrization of the STF- $\ell$  basis elements with the remaining  $(L - \ell)/2$  Kronecker symbols, naturally generalizing Eqs. (39)–(40):

$$F^{(\ell)}(\hat{\mathbf{n}}) = F_{i_1 \dots i_L}^{(\ell)} n_{i_1} \dots n_{i_L} = \sum_{m=-\ell}^{\ell} F^{\ell m} Y^{\ell m}(\hat{\mathbf{n}}). \quad (47)$$

The basis (46) of order- $L$  symmetric tensors is orthogonal with respect to taking the trace over all  $L$  indices.

To find all spherical tensor components  $F^{\ell m}$  for  $\ell = L, L - 2, \dots$  of a fully symmetric order- $L$  Cartesian tensor according to Eq. (45), in Supplementary Section S1 we generalize the normalization (43) for  $L > \ell$ :

$$\mathcal{Y}_{i_1 \dots i_L}^{\ell m*} \mathcal{Y}_{i_1 \dots i_L}^{\ell' m'} = \zeta(L, \ell) \delta_{\ell\ell'} \delta_{mm'}, \quad (48)$$

$$\zeta(L, \ell) = \frac{(L + \ell + 1)!!(L - \ell)!!}{L!(2\ell + 1)},$$

such that  $\zeta(\ell, \ell) = (2\ell - 1)!!/\ell!$  matches Eq. (43), yielding

$$F^{\ell m} = \frac{1}{\zeta(L, \ell)} \mathcal{Y}_{i_1 \dots i_L}^{\ell m*} \delta_{i_{\ell+1} i_{\ell+2}} \dots \delta_{i_{L-1} i_L} F_{i_1 \dots i_L}. \quad (49)$$

In other words, the degree- $\ell$  spherical tensor components  $F^{\ell m}$  in the decomposition (45) are obtained by taking the remaining  $(L - \ell)/2$  traces and convolving with the standard STF- $\ell$  basis element  $\mathcal{Y}_{i_1 \dots i_\ell}^{\ell m*}$ , albeit using the normalization coefficient  $1/\zeta(L, \ell)$  that “remembers” the original  $L > \ell$ .

So far, our discussion of  $\text{SO}(3)$  representations has been completely general. In dMRI context, every degree  $\ell$  is even due to time-reversal invariance of the Brownian motion, dictating even parity  $Y^{\ell m}(-\hat{\mathbf{n}}) = Y^{\ell m}(\hat{\mathbf{n}})$ . Hence, each cumulant or moment tensor, as in Eq. (1), can be split into a direct sum of irreducible representations with even  $\ell$  in Eq. (45), connecting it with the orientation dispersion in the SH basis [31, 88].

Applying the above methodology to the  $\mathbf{C}$  tensor, we first split it into  $\mathbf{S}$  and  $\mathbf{A}$ , Eq. (12)–(14). To decompose  $\mathbf{A}$ , we use Eqs. (15), where Eq. (15a) is  $A_{pq} = 4\Delta_{pq}$  from Eqs. (45)–(46) in [53]; here we use the same symbol  $\mathbf{A}$  for 2nd and 4th order tensors, as they are isomorphic (and represent the same geometric object). Eq. (15b) is obtained by using the identity

$\epsilon_{ijk}\epsilon_{lmn} = \delta_{il}\delta_{jm}\delta_{kn} + \delta_{im}\delta_{jn}\delta_{kl} + \delta_{in}\delta_{jl}\delta_{km} - \delta_{il}\delta_{jn}\delta_{km} - \delta_{in}\delta_{jm}\delta_{kl} - \delta_{im}\delta_{jl}\delta_{kn}$ . Eq. (15c) (the inverse relation) follows from  $\epsilon_{ijn}\epsilon_{klm} = \delta_{ik}\delta_{jl} - \delta_{il}\delta_{jk}$  and from the property  $A_{i(jkl)} \equiv 0$  that is a consequence of Eq. (14).

Now that all Cartesian tensors  $S_{ijkl}$  and  $A_{pq}$  derived from  $C$  are fully symmetric, we can represent them as combinations of spherical tensors, cf. Eq. (45). Applying Eq. (49), we get

$$\begin{aligned} D^{00} &= \frac{1}{3} D_{ii} & D^{2m} &= \frac{2}{3} \mathcal{Y}_{ij}^{2m*} D_{ij}; \\ A^{00} &= \frac{1}{3} A_{ii}, & A^{2m} &= \frac{2}{3} \mathcal{Y}_{ij}^{2m*} A_{ij}; \\ S^{00} &= \frac{1}{5} S_{iiij}, & S^{2m} &= \frac{4}{7} \mathcal{Y}_{ij}^{2m*} S_{ijkk}, \\ & & S^{4m} &= \frac{8}{35} \mathcal{Y}_{ijkl}^{4m*} S_{ijkl}. \end{aligned} \quad (50)$$

Eqs. (18) then relate the components (50) to those of  $Q$  and  $T$ .

### From tissue diffusivities to QT decomposition

We derived Eqs. (18) using a shortcut that happens to work for the  $C$  tensor: the special  $B$ -tensor family (9) allowed us to match the SH components (10) with those of Eqs. (17). It turns out that for higher-order tensors (arising at the  $O(b^3)$  level and beyond), the axially-symmetric family (9) does not probe all their dof. Hence, below we provide a more generalizable way to derive Eqs. (18) by explicitly following the components (50) through triple products of SH and the corresponding Clebsch-Gordan coefficients. This highlights the connection between the compartmental diffusion tensor covariances and the addition of angular momenta (cf. Supplementary Section S2).

We begin from the irreducible decomposition of compartmental diffusion tensors (3), this can be used to explicitly write  $D$  and  $C$ , Eqs. (2):

$$\begin{aligned} D_{ij} &= \langle D^{00} \rangle \delta_{ij} + \sum_m \langle D^{2m} \rangle \mathcal{Y}_{ij}^{2m}, \\ C_{ijkl} &= \langle (D^{00})^2 \rangle \delta_{ij}\delta_{kl} + \sum_{m,m'} \langle \langle D^{2m} D^{2m'} \rangle \rangle \mathcal{Y}_{ij}^{2m} \mathcal{Y}_{kl}^{2m'} \\ &+ \sum_m \langle \langle D^{00} D^{2m} \rangle \rangle \left( \delta_{ij} \mathcal{Y}_{kl}^{2m} + \mathcal{Y}_{ij}^{2m} \delta_{kl} \right) \end{aligned} \quad (51)$$

The SA decomposition of  $C$ , Eqs. (12)-(14), yields

$$\begin{aligned} S_{ijkl} &= \langle (D^{00})^2 \rangle \delta_{(ij}\delta_{kl)} + 2 \sum_m \langle \langle D^{00} D^{2m} \rangle \rangle \delta_{(ij} \mathcal{Y}_{kl)}^{2m} \\ &+ \sum_{m,m'} \langle \langle D^{2m} D^{2m'} \rangle \rangle \mathcal{Y}_{(ij}^{2m} \mathcal{Y}_{kl)}^{2m'}, \\ A_{ijkl} &= C_{ijkl} - S_{ijkl} = \langle (D^{00})^2 \rangle \left( \delta_{ij}\delta_{kl} - \delta_{(ij}\delta_{kl)} \right) \\ &+ \sum_m \langle \langle D^{00} D^{2m} \rangle \rangle \left( \delta_{ij} \mathcal{Y}_{kl}^{2m} + \mathcal{Y}_{ij}^{2m} \delta_{kl} - 2\delta_{(ij} \mathcal{Y}_{kl)}^{2m} \right) \\ &+ \sum_{m,m'} \langle \langle D^{2m} D^{2m'} \rangle \rangle \left( \mathcal{Y}_{ij}^{2m} \mathcal{Y}_{kl}^{2m'} - \mathcal{Y}_{(ij}^{2m} \mathcal{Y}_{kl)}^{2m'} \right). \end{aligned}$$

Although  $A_{ijkl}$  does not seem to have any particular symmetry at first glance, it can be mapped to a second order symmetric

tensor using Eq. (15b):

$$\begin{aligned} A_{pq} &= \delta_{pq} (A_{iikk} - A_{ikik}) + 2(A_{pkqk} - A_{pqkk}) \\ &= 2 \langle \langle (D^{00})^2 \rangle \rangle \delta_{pq} - 2 \sum_m \langle \langle D^{00} D^{2m} \rangle \rangle \mathcal{Y}_{pq}^{2m} \\ &- \sum_{m,m'} \langle \langle D^{2m} D^{2m'} \rangle \rangle \left( \mathcal{Y}_{ij}^{2m} \mathcal{Y}_{ij}^{2m'} \delta_{pq} - 2 \mathcal{Y}_{pk}^{2m} \mathcal{Y}_{qk}^{2m'} \right). \end{aligned}$$

This leaves us with symmetric tensors  $D_{ij}$ ,  $S_{ijkl}$ , and  $A_{pq}$  written as a function of compartmental diffusion tensor covariances, for which we can compute irreducible decompositions following Eqs. (50). Below we group their spherical tensor elements according to their degree  $\ell$ :

$$\begin{aligned} D^{00} &= \langle \langle D^{00} \rangle \rangle, \\ S^{00} &= \langle \langle (D^{00})^2 \rangle \rangle + \frac{1}{5} \sum_{m',m''} \langle \langle D^{2m'} D^{2m''} \rangle \rangle \mathcal{Y}_{(ij}^{2m'} \mathcal{Y}_{kl)}^{2m''} \mathcal{Y}_{ijkl}^{00*}, \\ A^{00} &= 2 \langle \langle (D^{00})^2 \rangle \rangle - \frac{1}{2} \sum_{m',m''} \langle \langle D^{2m'} D^{2m''} \rangle \rangle \mathcal{Y}_{(ij}^{2m'} \mathcal{Y}_{kl)}^{2m''} \mathcal{Y}_{ijkl}^{00*}, \\ D^{2m} &= \langle \langle D^{2m} \rangle \rangle, \\ S^{2m} &= 2 \langle \langle D^{00} D^{2m} \rangle \rangle + \frac{4}{7} \sum_{m',m''} \langle \langle D^{2m'} D^{2m''} \rangle \rangle \mathcal{Y}_{(ij}^{2m'} \mathcal{Y}_{kl)}^{2m''} \mathcal{Y}_{ijkl}^{2m*}, \\ A^{2m} &= -2 \langle \langle D^{00} D^{2m} \rangle \rangle + 2 \sum_{m',m''} \langle \langle D^{2m'} D^{2m''} \rangle \rangle \mathcal{Y}_{(ij}^{2m'} \mathcal{Y}_{kl)}^{2m''} \mathcal{Y}_{ijkl}^{2m*}, \\ S^{4m} &= \frac{8}{35} \sum_{m',m''} \langle \langle D^{2m'} D^{2m''} \rangle \rangle \mathcal{Y}_{(ij}^{2m'} \mathcal{Y}_{kl)}^{2m''} \mathcal{Y}_{ijkl}^{4m*}, \end{aligned} \quad (52)$$

using  $\mathcal{Y}_{ij}^{2m} \mathcal{Y}_{ij}^{2m'} = \frac{3}{2} \mathcal{Y}_{(ij}^{2m} \mathcal{Y}_{kl)}^{2m'} \mathcal{Y}_{ijkl}^{00}$  and  $\mathcal{Y}_{ij}^{2m'} \mathcal{Y}_{jk}^{2m''} \mathcal{Y}_{ki}^{2m*} = \frac{3}{2} \mathcal{Y}_{(ij}^{2m'} \mathcal{Y}_{kl)}^{2m''} \mathcal{Y}_{ijkl}^{2m*}$ .

The connection (18) to the QT decomposition (8) is established via the relations of the triple products of spherical basis tensors to the products of Clebsch-Gordan coefficients:

$$\begin{aligned} \mathcal{Y}_{(ij}^{2m'} \mathcal{Y}_{kl)}^{2m''} \mathcal{Y}_{ijkl}^{00*} &= 5 \langle 2020|00 \rangle \langle 2m' 2m''|00 \rangle, \\ \mathcal{Y}_{(ij}^{2m'} \mathcal{Y}_{kl)}^{2m''} \mathcal{Y}_{ijkl}^{2m*} &= \frac{7}{4} \langle 2020|20 \rangle \langle 2m' 2m''|2m \rangle, \\ \mathcal{Y}_{(ij}^{2m'} \mathcal{Y}_{kl)}^{2m''} \mathcal{Y}_{ijkl}^{4m*} &= \frac{35}{8} \langle 2020|40 \rangle \langle 2m' 2m''|4m \rangle, \end{aligned} \quad (53)$$

see derivation of the Supplementary Eq. (53). We then use Eq. (8b) to express the sums in Eqs. (52) via  $T^{\ell m}$ :

$$\begin{aligned} \sum_{m',m''} \langle \langle D^{2m'} D^{2m''} \rangle \rangle \mathcal{Y}_{(ij}^{2m'} \mathcal{Y}_{kl)}^{2m''} \mathcal{Y}_{ijkl}^{00*} &= 5T^{00}, \\ \sum_{m',m''} \langle \langle D^{2m'} D^{2m''} \rangle \rangle \mathcal{Y}_{(ij}^{2m'} \mathcal{Y}_{kl)}^{2m''} \mathcal{Y}_{ijkl}^{2m*} &= \frac{7}{4}T^{2m}, \\ \sum_{m',m''} \langle \langle D^{2m'} D^{2m''} \rangle \rangle \mathcal{Y}_{(ij}^{2m'} \mathcal{Y}_{kl)}^{2m''} \mathcal{Y}_{ijkl}^{4m*} &= \frac{35}{8}T^{4m}, \end{aligned} \quad (54)$$

which after simple algebra proves the system (18).

At first glance, Clebsch-Gordan coefficients may seem a non-intuitive way to combine the components  $\langle \langle D^{2m'} D^{2m''} \rangle \rangle$ . However, they can yield elegant simplifications. Consider  $T^{00}$  as defined in Eq. (8b). Using  $\langle 2020|00 \rangle = 1/\sqrt{5}$  and  $\langle 2m 2m'|00 \rangle = (-1)^m \delta_{m,-m'}/\sqrt{5}$ , as well as Eq. (42), we get

$$\begin{aligned} T^{00} &= \langle 2020|00 \rangle \sum_{m,m'} \langle 2m 2m'|00 \rangle \langle \langle D^{2m} D^{2m'} \rangle \rangle \\ &= \frac{1}{5} \sum_m (-1)^m \langle \langle D^{2m} D^{2-m} \rangle \rangle = \frac{1}{5} \sum_m \langle \langle D^{2m} D^{2m*} \rangle \rangle. \end{aligned} \quad (55)$$

### Intrinsic invariants of $\mathbb{T}^{(4)} = \mathbb{S}^{(4)}$

The 3 independent invariants for a 2nd-order tensor, such as  $\mathbb{D}$ , can be constructed from the coefficients of its characteristic polynomial  $p(\lambda) = \det(\mathbb{D} - \lambda \mathbb{I}) = -\lambda^3 + c_2 \lambda^2 + c_1 \lambda + c_0$ ;  $c_0 = \det \mathbb{D}$ ,  $c_1 = \frac{1}{2}(\text{tr} \mathbb{D}^2 - \text{tr}^2 \mathbb{D})$ , and  $c_2 = \text{tr} \mathbb{D}$ . In the main text, we mapped them onto  $\mathbb{D}_0$ ,  $\mathbb{D}_2$ , and  $\mathbb{D}_{2|3}$ , Eqs. (5) and (21), by first isolating the scalar and the STF-2 parts, Eq. (3).

For 4th-order tensors, the characteristic polynomial needs to be defined. Fortunately, 4th-order 3d tensors with minor symmetry, like the elasticity or covariance tensors, can be mapped to a 2nd-order 6d tensor  $\mathbb{C} \rightarrow \mathbb{C}_{6 \times 6}$  using the Kelvin/Mandel notation [42, 56]. Explicitly [56]:

$$\mathbb{C}_{6 \times 6} = \begin{pmatrix} \mathbb{C}_{1111} & \mathbb{C}_{1122} & \mathbb{C}_{1133} & \sqrt{2} \mathbb{C}_{1112} & \sqrt{2} \mathbb{C}_{1113} & \sqrt{2} \mathbb{C}_{1123} \\ \mathbb{C}_{1122} & \mathbb{C}_{2222} & \mathbb{C}_{2233} & \sqrt{2} \mathbb{C}_{2212} & \sqrt{2} \mathbb{C}_{2213} & \sqrt{2} \mathbb{C}_{2223} \\ \mathbb{C}_{1133} & \mathbb{C}_{2233} & \mathbb{C}_{3333} & \sqrt{2} \mathbb{C}_{3312} & \sqrt{2} \mathbb{C}_{3313} & \sqrt{2} \mathbb{C}_{3323} \\ \sqrt{2} \mathbb{C}_{1112} & \sqrt{2} \mathbb{C}_{2212} & \sqrt{2} \mathbb{C}_{3312} & 2 \mathbb{C}_{1212} & 2 \mathbb{C}_{1213} & 2 \mathbb{C}_{1223} \\ \sqrt{2} \mathbb{C}_{1113} & \sqrt{2} \mathbb{C}_{2213} & \sqrt{2} \mathbb{C}_{3313} & 2 \mathbb{C}_{1312} & 2 \mathbb{C}_{1313} & 2 \mathbb{C}_{1323} \\ \sqrt{2} \mathbb{C}_{1123} & \sqrt{2} \mathbb{C}_{2223} & \sqrt{2} \mathbb{C}_{3323} & 2 \mathbb{C}_{2312} & 2 \mathbb{C}_{2313} & 2 \mathbb{C}_{2323} \end{pmatrix}, \quad (56)$$

where the major symmetry of  $\mathbb{C}$  makes  $\mathbb{C}_{6 \times 6}$  symmetric, and factors  $\sqrt{2}$  and 2 account for repeated elements, such that we can define traces of the powers of 4th-order tensors as

$$\text{tr} \mathbb{C}^n \equiv \mathbb{C}_{i_1 j_1 i_2 j_2} \dots \mathbb{C}_{i_n j_n i_1 j_1} = \text{tr} (\mathbb{C}_{6 \times 6})^n. \quad (57)$$

The mapping  $\mathbb{C} \rightarrow \mathbb{C}_{6 \times 6}$  allows one to extract 6 invariants from the characteristic polynomial of a square matrix  $\mathbb{C}_{6 \times 6}$ . This approach was extended [42] by considering the coefficients of the polynomial  $\tilde{p}(\lambda, \mu) = \det (\mathbb{C}_{6 \times 6} - \lambda \mathbb{I} - \mu \mathbb{I}^{(4)})$  with  $\mathbb{I}_{ijkl}^{(4)}(\lambda, \mu) = \frac{\lambda}{2}(\delta_{ik} \delta_{jl} + \delta_{il} \delta_{jk}) + \mu \delta_{ij} \delta_{kl}$ . However, such invariants do not form a complete set, and besides, they mix the irreducible representations and symmetries.

The irreducible decomposition (6) allows us to keep track of symmetries, and consider a more constrained problem: find the 6 intrinsic invariants of the only component  $\mathbb{S}^{(4)} = \mathbb{T}^{(4)}$  of  $\mathbb{C}$  that is neither a scalar nor an STF-2 tensor. For that, we use the mapping (56) to define a  $6 \times 6$  matrix  $\mathbb{S}_{6 \times 6}^{(4)}$ , cf. Supplementary Eq. (S20). We consider standard characteristic polynomial  $p(\lambda) = \det (\mathbb{S}_{6 \times 6}^{(4)} - \lambda \mathbb{I})$  because, as it turns out, no extra invariants arise from the coefficients of  $\tilde{p}(\lambda, \mu)$  for  $\mathbb{S}_{6 \times 6}^{(4)}$ .

From direct inspection of  $\mathbb{S}_{6 \times 6}^{(4)}$  (Supplementary Section S4) we find that its trace and one of its eigenvalues are zero. The polynomial  $p(\lambda) = \lambda^6 + p_5 \lambda^5 + \dots + p_1 \lambda + p_0$  has only 4 algebraically independent coefficients:

$$\begin{aligned} p_1 &= \frac{1}{6} \text{tr} (\mathbb{S}^{(4)})^2 \text{tr} (\mathbb{S}^{(4)})^3 - \frac{1}{5} \text{tr} (\mathbb{S}^{(4)})^5, \\ p_2 &= \frac{1}{8} \text{tr} (\mathbb{S}^{(4)})^2 \text{tr} (\mathbb{S}^{(4)})^2 - \frac{1}{4} \text{tr} (\mathbb{S}^{(4)})^4, \\ p_3 &= -\frac{1}{3} \text{tr} (\mathbb{S}^{(4)})^3, \\ p_4 &= -\frac{1}{2} \text{tr} (\mathbb{S}^{(4)})^2, \end{aligned} \quad (58)$$

since  $p_0 = \det \mathbb{S}_{6 \times 6}^{(4)} = 0$  and  $p_5 = -\text{tr} \mathbb{S}^{(4)} = 0$  (traces are defined according to Eq. (57)). Thus  $p(\lambda)$  has 4 nonzero

independent roots (eigenvalues of  $\mathbb{S}_{6 \times 6}^{(4)}$ ). Since by Cayley–Hamilton theorem, each matrix satisfies its characteristic equation,  $p(\mathbb{S}_{6 \times 6}^{(4)}) = 0$ , the 4 traces  $\text{tr} (\mathbb{S}^{(4)})^2$ ,  $\text{tr} (\mathbb{S}^{(4)})^3$ ,  $\text{tr} (\mathbb{S}^{(4)})^4$ , and  $\text{tr} (\mathbb{S}^{(4)})^5$ , are the 4 algebraically independent invariants that determine all traces of higher powers of  $\mathbb{S}^{(4)}$ . The latter can be iteratively obtained from relations  $\text{tr} [(\mathbb{S}^{(4)})^n p(\mathbb{S}^{(4)})] = 0$ ,  $n = 0, 1, 2, \dots$ , by expressing  $\text{tr} (\mathbb{S}^{(4)})^{6+n}$  via the above 4 independent traces that also define the characteristic polynomial coefficients, Eq. (58).

The remaining 2 independent intrinsic invariants of  $\mathbb{S}^{(4)}$  can be obtained from its eigentensor decomposition [56]

$$\mathbb{S}_{ijkl}^{(4)} = \sum_{a=1}^6 \lambda_a \mathbb{E}_{ij}^{(a)} \mathbb{E}_{kl}^{(a)}, \quad (59)$$

where  $\lambda_a$  and  $\mathbb{E}_{ij}^{(a)}$  are the eigenvalues and eigentensors of  $\mathbb{S}^{(4)}$  according to the mapping (56). Namely,  $\lambda_a$  are the eigenvalues of  $\mathbb{S}_{6 \times 6}^{(4)}$ , and  $\hat{\mathbf{v}}^{(a)} = [v_{xx}^{(a)}, v_{yy}^{(a)}, v_{zz}^{(a)}, v_{xy}^{(a)}, v_{xz}^{(a)}, v_{yz}^{(a)}]$  are its normalized 6d eigenvectors, yielding the eigentensors

$$\mathbb{E}_{ij}^{(a)} = \begin{pmatrix} v_{xx}^{(a)} & \frac{1}{\sqrt{2}} v_{xy}^{(a)} & \frac{1}{\sqrt{2}} v_{xz}^{(a)} \\ \frac{1}{\sqrt{2}} v_{xy}^{(a)} & v_{yy}^{(a)} & \frac{1}{\sqrt{2}} v_{yz}^{(a)} \\ \frac{1}{\sqrt{2}} v_{xz}^{(a)} & \frac{1}{\sqrt{2}} v_{yz}^{(a)} & v_{zz}^{(a)} \end{pmatrix}. \quad (60)$$

The orthogonality of  $\hat{\mathbf{v}}^{(a)}$  induces the tensor orthogonality  $\mathbb{E}_{ij}^{(a)} \mathbb{E}_{ij}^{(b)} = \delta_{ab}$ . Based on Supplementary Section S4, the eigenvector  $\hat{\mathbf{v}}^{(a_0)} = \frac{1}{\sqrt{3}}(1, 1, 1, 0, 0, 0)^t$ , associated with a zero eigenvalue  $\lambda_{a_0} = 0$ , corresponds to the eigentensor

$$\mathbb{E}_{ij}^{(a_0)} = \frac{1}{\sqrt{3}} \delta_{ij}; \quad \text{tr} \mathbb{E}^{(a)} = 0, \quad a \neq a_0, \quad (61)$$

with the latter equality for all other 5 eigentensors stemming from their orthogonality to  $\mathbb{E}^{(a_0)}$ . Note that, although the tensor products  $\mathbb{E}_{ij}^{(a)} \mathbb{E}_{kl}^{(a)}$  are not fully symmetric, when combined according to Eq. (59),  $\mathbb{S}_{ijkl}^{(4)}$  becomes fully symmetric.

We now define the remaining 2 independent invariants of  $\mathbb{S}^{(4)}$  by arranging the above eigentensors into the following 2 combinations:

$$\mathbb{E}_{ij} = \sum_{a=1}^6 \lambda_a \mathbb{E}_{ij}^{(a)}, \quad \text{and} \quad \tilde{\mathbb{E}}_{ij} = \sum_{a \neq a_0} \mathbb{E}_{ij}^{(a)}. \quad (62)$$

Analogously to the D-tensor example above, traces of the powers of 2nd-order tensors  $\mathbb{E}$  and  $\tilde{\mathbb{E}}$  are rotationally invariant; the traces of 1st, 2nd and 3rd powers of these matrices are algebraically independent. Further, by construction,  $\text{tr} \mathbb{E} = \text{tr} \tilde{\mathbb{E}} = 0$ . One can also check that  $\text{tr} \mathbb{E}^2 = \text{tr} (\mathbb{S}^{(4)})^2$  given by one of the previously found invariants, and  $\text{tr} \tilde{\mathbb{E}}^2 = 5$  independent of  $\mathbb{S}^{(4)}$ . Therefore, we identify the two remaining independent intrinsic invariants of  $\mathbb{S}^{(4)}$  with  $\text{tr} \mathbb{E}^3$  and  $\text{tr} \tilde{\mathbb{E}}^3$ . To summarize, the 6 intrinsic invariants of  $\mathbb{S}^{(4)}$  are:

$$\begin{aligned} \mathbb{S}_{4|n} &= \left( \frac{8}{35} \text{tr} (\mathbb{S}^{(4)})^n \right)^{1/n}, \quad n = 2 \dots 5; \\ \mathbb{S}_{4|6} &= \text{tr}^{1/3} \mathbb{E}^3, \quad \mathbb{S}_{4|7} = \text{tr}^{1/3} \tilde{\mathbb{E}}^3, \end{aligned} \quad (63)$$

with  $\mathbb{E}$  and  $\tilde{\mathbb{E}}$  defined in Eq. (62). They are normalized such that  $\mathbb{S}_4 \equiv \mathbb{S}_{4|2}$  is the 2-norm of  $\mathbb{S}^{4m}$ , cf. Eq. (24).

TABLE II. Description of the four protocols (rows) acquired for each volunteer. Imaging parameters were kept constant for all protocols and numbers denote the different directions sampled on each shell. All b-values are in microstructure units  $\text{ms}/\mu\text{m}^2$ .

Resolution = $2 \times 2 \times 2 \text{ mm}^3$ , PF = 6/8, $R_{\text{GRAPPA}} = 2$ , 68 slices, MB=2, TE=90ms, TR=4.2s						
Protocol	$b = 0$	$b_{\text{LTE}} = 1$	$b_{\text{LTE}} = 2$	$b_{\text{PTE}} = 1.5$	$b_{\text{STE}} = 1.5$	$t_{\text{acq}}$ [min' sec'']
DKI	1	30	60	-	-	6' 43''
iRICE (MD+FA+MK)	1	6	6	-	-	1' 14''
RICE	2	30	60	30	-	11' 20''
iRICE (MD+FA+MK+ $\mu$ FA)	2	6	6	-	3	1' 56''

### MRI experiments

After providing informed consent, three healthy volunteers (23 yo female, 25 yo female, 33 yo male) underwent MRI in a whole body 3T-system (Siemens, Prisma) using a 32-channel head coil. Maxwell-compensated free gradient diffusion waveforms [89] were used to yield linear, planar, and spherical B-tensor encoding using a prototype spin echo sequence with EPI read-out [90]. Four diffusion datasets were acquired according to Table II. Imaging parameters: voxel size =  $2 \times 2 \times 2 \text{ mm}^3$ ,  $T_R = 4.2 \text{ s}$ ,  $T_E = 90 \text{ ms}$ , bandwidth = 1818 Hz/Px,  $R_{\text{GRAPPA}} = 2$ , partial Fourier = 6/8, multiband = 2. Total scan time was approximately 15 minutes per subject for all protocols.

### Image pre-processing

All four protocols in Table II were processed identically and independently for each subject. Magnitude and phase data were reconstructed. Then, a phase estimation and unwinding step preceded the denoising of the complex images [91]. Denoising was done using the Marchenko-Pastur principal component analysis method [92] on the real part of the phase-unwinded data. An advantage of denoising before taking the magnitude of the data is that Rician bias is reduced significantly [62]. We also processed this data using only magnitude data. Here, magnitude denoising and Rician bias correction were applied, see results in Supplementary Section S7. Data was subsequently processed with the DESIGNER pipeline [93]. Denoised images were corrected for Gibbs ringing artifacts accounting for the partial Fourier acquisition [94], based on re-sampling images using local sub-voxel shifts. Images were then rigidly aligned and corrected for eddy current distortions and subject motion simultaneously [95]. A  $b = 0$  image with reverse phase encoding was included for correction of EPI-induced distortions [96]. Finally, MRI voxels were locally smoothed based on spatial and intensity similarity akin [97].

### Parameter estimation

Two variants of the cumulant expansion were fit to the four datasets described in Table II. This depended on which parameters each protocol was sensitive to. The full DKI and full RICE protocols were fit to Eq. (10) while the minimal DKI and minimal RICE protocols were fit to Eq. (33). Weighted linear least squares were used for fitting [98] to highlight the

gain achieved purely by acquisition optimization. Including positivity constraints to improve parameters robustness [99] is straightforward in spherical tensor parametrization but is outside of the scope of this work. All codes for RICE parameter estimation were implemented in MATLAB (R2021a, MathWorks, Natick, Massachusetts). These are publicly available together with an anonymized dataset as part of the RICE toolbox at <https://github.com/NYU-DiffusionMRI/RICE>.

### ACKNOWLEDGMENTS

This work was performed under the rubric of the Center for Advanced Imaging Innovation and Research (CAI<sup>2</sup>R, <https://www.cai2r.net>), an NIBIB Biomedical Technology Resource Center NIH P41-EB017183 (DN, EF). This work has been supported by NIH under NINDS R01 NS088040 (DN, EF) and NIBIB R01 EB027075 (DN, EF) and K99 EB036080 (SC) awards, as well as by the Swedish Research Council 2021-04844 (FS) and the Swedish Cancer Society 22 0592 JIA (FS)). Authors are grateful to Sune Jespersen, Valerij Kiselev and Jelle Veraart for fruitful discussions.

### CONFLICT OF INTEREST STATEMENT

SC, EF, DSN are co-inventors in technology related to this research; a PCT patent application is pending. EF, DSN, and NYU School of Medicine are stock holders of Microstructure Imaging, Inc. — post-processing tools for advanced MRI methods. FS is an inventor of technology related to this research and has financial interest in related patents.

- [1] P. T. Callaghan, *Principles of Nuclear Magnetic Resonance Microscopy*, Oxford Science Publications (Clarendon, 1991).
- [2] D. K. Jones, *Diffusion MRI* (Oxford University Press, 2010).
- [3] P. J. Basser, J. Mattiello, and D. LeBihan, Estimation of the effective self-diffusion tensor from the NMR spin echo, *Journal of Magnetic Resonance* **103**, 247 (1994).
- [4] I. O. Jelescu and M. D. Budde, Design and validation of diffusion MRI models of white matter, *Frontiers in Physics* **5**, 61 (2017).
- [5] D. S. Novikov, E. Fieremans, S. N. Jespersen, and V. G. Kiselev, Quantifying brain microstructure with diffusion MRI: Theory and parameter estimation, *NMR in Biomedicine*, e3998 (2019).
- [6] D. C. Alexander, T. B. Dyrby, M. Nilsson, and H. Zhang, Imaging brain microstructure with diffusion MRI: practicality and applications, *NMR in Biomedicine* **32**, e3841 (2019).
- [7] D. S. Novikov, The present and the future of microstructure MRI: From a paradigm shift to normal science, *Journal of Neuroscience Methods* **351**, 108947 (2021).
- [8] V. G. Kiselev, Microstructure with diffusion MRI: what scale we are sensitive to?, *Journal of Neuroscience Methods* **347**, 108910 (2021).
- [9] N. Weiskopf, L. J. Edwards, G. Helms, S. Mohammadi, and E. Kirilina, Quantitative magnetic resonance imaging of brain anatomy and in vivo histology, *Nature Reviews Physics* **3**, 570 (2021).
- [10] B. Lampinen, F. Szczepankiewicz, J. Lätt, L. Knutsson, J. Mårtensson, I. M. Björkman-Burtscher, D. van Westen, P. C. Sundgren, F. Ståhlberg, and M. Nilsson, Probing brain tissue microstructure with mri: principles, challenges, and the role of multidimensional diffusion-relaxation encoding, *NeuroImage* **282**, 120338 (2023).
- [11] Y. Assaf, Can we use diffusion MRI as a bio-marker of neurodegenerative processes?, *BioEssays* **30**, 1235 (2008).
- [12] M. Nilsson, E. Englund, F. Szczepankiewicz, D. van Westen, and P. C. Sundgren, Imaging brain tumour microstructure, *NeuroImage* **182**, 232 (2018), microstructural Imaging.
- [13] D. S. Novikov, J. H. Jensen, J. A. Helpert, and E. Fieremans, Revealing mesoscopic structural universality with diffusion., *Proceedings of the National Academy of Sciences of the United States of America* **111**, 5088 (2014).
- [14] V. G. Kiselev, Fundamentals of diffusion MRI physics, *NMR in Biomedicine* **30**, 1 (2017).
- [15] D. G. Cory, A. N. Garroway, and J. B. Miller, Applications of spin transport as a probe of local geometry, *Polymer Preprints* **31**, 149 (1990).
- [16] P. P. Mitra, Multiple wave-vector extensions of the NMR pulsed-field-gradient spin-echo diffusion measurement, *Physical Review B* **51**, 15074 (1995).
- [17] S. Mori and P. C. M. Van Zijl, Diffusion weighting by the trace of the diffusion tensor within a single scan, *Magnetic Resonance in Medicine* **33**, 41 (1995).
- [18] N. Shemesh, S. N. Jespersen, D. C. Alexander, Y. Cohen, I. Drobnjac, T. B. Dyrby, J. Finterbusch, M. A. Koch, T. Kuder, F. Laun, M. Lawrenz, H. Lundell, P. P. Mitra, M. Nilsson, E. Özarslan, D. Topgaard, and C.-F. Westin, Conventions and nomenclature for Double Diffusion Encoding NMR and MRI, *Magnetic Resonance in Medicine* **75**, 82 (2015).
- [19] C.-F. Westin, H. Knutsson, O. Pasternak, F. Szczepankiewicz, E. Özarslan, D. van Westen, C. Mattisson, M. Bogren, L. J. O'Donnell, M. Kubicki, D. Topgaard, and M. Nilsson, q-space trajectory imaging for multidimensional diffusion MRI of the human brain, *NeuroImage* **135**, 345 (2016).
- [20] D. Topgaard, Multidimensional diffusion MRI, *Journal of Magnetic Resonance* **275**, 98 (2017).
- [21] N. G. van Kampen, *Stochastic Processes in Physics and Chemistry*, 1st ed. (Elsevier, Oxford, 1981).
- [22] V. G. Kiselev, The cumulant expansion: an overarching mathematical framework for understanding diffusion NMR, in *Diffusion MRI: Theory, Methods and Applications*, edited by D. K. Jones (Oxford University Press, Oxford, 2010) Chap. 10, pp. 152–168.
- [23] S. N. Jespersen, H. Lundell, C. K. Sønderby, and T. B. Dyrby, Orientationally invariant metrics of apparent compartment eccentricity from double pulsed field gradient diffusion experiments, *NMR in Biomedicine* **26**, 1647 (2013).
- [24] R. N. Henriques, S. N. Jespersen, and N. Shemesh, Correlation tensor magnetic resonance imaging, *NeuroImage* **211**, 116605 (2020).
- [25] S. Desmond-Hellmann, Toward precision medicine: A new social contract?, *Science Translational Medicine* **4**, 129ed3 (2012).
- [26] M. Kazhdan, T. Funkhouser, and S. Rusinkiewicz, Rotation invariant spherical harmonic representation of 3d shape descriptors, in *Proceedings of the 2003 Eurographics/ACM SIGGRAPH Symposium on Geometry Processing*, SGP 03 (Eurographics Association, 2003) pp. 156–164.
- [27] B. Gutman, Y. Wang, L. M. Lui, T. F. Chan, and P. M. Thompson, Hippocampal surface discrimination via invariant descriptors of spherical conformal maps, in *2007 4th IEEE International Symposium on Biomedical Imaging: From Nano to Macro* (2007) pp. 1316–1319.
- [28] H. Mirzaalian, L. Ning, P. Savadjiev, O. Pasternak, S. Bouix, O. Michailovich, G. Grant, C. Marx, R. Morey, L. Flashman, M. George, T. McAllister, N. Andaluz, L. Shutter, R. Coimbra, R. Zafonte, M. Coleman, M. Kubicki, C. Westin, M. Stein, M. Shenton, and Y. Rathi, Inter-site and inter-scanner diffusion mri data harmonization, *NeuroImage* **135**, 311 (2016).
- [29] M. Reisert, E. Kellner, B. Dhital, J. Hennig, and V. G. Kiselev, Disentangling micro from mesostructure by diffusion MRI: A Bayesian approach, *NeuroImage* **147**, 964 (2017).
- [30] H. Skibbe and M. Reisert, Spherical Tensor Algebra: A Toolkit for 3D Image Processing, *Journal of Mathematical Imaging and Vision* **58**, 349 (2017).
- [31] D. S. Novikov, J. Veraart, I. O. Jelescu, and E. Fieremans, Rotationally-invariant mapping of scalar and orientational metrics of neuronal microstructure with diffusion MRI, *NeuroImage* **174**, 518 (2018).
- [32] M. Reisert, V. A. Coenen, C. Kaller, K. Egger, and H. Skibbe, HAMLET: Hierarchical harmonic filters for learning tracts from diffusion mri (2018), [arXiv:1807.01068 \[cs.CV\]](https://arxiv.org/abs/1807.01068).
- [33] S. M. Smith, G. Douaud, W. Chen, T. Hanayik, F. Alfaro-Almagro, K. Sharp, and L. T. Elliott, An expanded set of genome-wide association studies of brain imaging phenotypes in UK Biobank, *Nature Neuroscience* **24**, 737 (2021).
- [34] C. R. Jack Jr., M. A. Bernstein, N. C. Fox, P. Thompson, G. Alexander, D. Harvey, B. Borowski, P. J. Britson, J. L. Whitwell, C. Ward, A. M. Dale, J. P. Felmlee, J. L. Gunter, D. L. Hill, R. Killiany, N. Schuff, S. Fox-Bosetti, C. Lin, C. Studholme, C. S. DeCarli, G. Krueger, H. A. Ward, G. J. Metzger, K. T. Scott, R. Mallozzi, D. Blezek, J. Levy, J. P. Debbins, A. S. Fleisher, M. Albert, R. Green, G. Bart-

- zokis, G. Glover, J. Mugler, and M. W. Weiner, The alzheimer's disease neuroimaging initiative (adni): Mri methods, *Journal of Magnetic Resonance Imaging* **27**, 685 (2008).
- [35] N. Jahanshad, P. V. Kochunov, E. Sprooten, R. C. Mandl, T. E. Nichols, L. Almasy, J. Blangero, R. M. Brouwer, J. E. Curran, G. I. de Zubicaray, R. Duggirala, P. T. Fox, L. E. Hong, B. A. Landman, N. G. Martin, K. L. McMahon, S. E. Medland, B. D. Mitchell, R. L. Olvera, C. P. Peterson, J. M. Starr, J. E. Sussmann, A. W. Toga, J. M. Wardlaw, M. J. Wright, H. E. Hulshoff Pol, M. E. Bastin, A. M. McIntosh, I. J. Deary, P. M. Thompson, and D. C. Glahn, Multi-site genetic analysis of diffusion images and voxelwise heritability analysis: A pilot project of the enigma-dti working group, *NeuroImage* **81**, 455 (2013).
- [36] M. F. Glasser, S. M. Smith, D. S. Marcus, J. L. R. Andersson, E. J. Auerbach, T. E. J. Behrens, T. S. Coalson, M. P. Harms, M. Jenkinson, S. Moeller, E. C. Robinson, S. N. Sotiropoulos, J. Xu, E. Yacoub, K. Ugurbil, and D. C. Van Essen, The human connectome project's neuroimaging approach, *Nature Neuroscience* **19**, 1175 (2016).
- [37] K. L. Miller, F. Alfaro-Almagro, N. K. Bangerter, D. L. Thomas, E. Yacoub, J. Xu, A. J. Bartsch, S. Jbabdi, S. N. Sotiropoulos, J. L. R. Andersson, L. Griffanti, G. Douaud, T. W. Okell, P. Weale, I. Dragonu, S. Garratt, S. Hudson, R. Collins, M. Jenkinson, P. M. Matthews, and S. M. Smith, Multimodal population brain imaging in the UK Biobank prospective epidemiological study, *Nature Neuroscience* **19**, 1523 (2016).
- [38] N. D. Volkow, G. F. Koob, R. T. Croyle, D. W. Bianchi, J. A. Gordon, W. J. Koroshetz, E. J. Perez-Stable, W. T. Riley, M. H. Bloch, K. Conway, B. G. Deeds, G. J. Dowling, S. Grant, K. D. Howlett, J. A. Matochik, G. D. Morgan, M. M. Murray, A. Noronha, C. Y. Spong, E. M. Wargo, K. R. Warren, and S. R. Weiss, The conception of the abcd study: From substance use to a broad nih collaboration, *Developmental Cognitive Neuroscience* **32**, 4 (2018).
- [39] J. R. Taylor, N. Williams, R. Cusack, T. Auer, M. A. Shafto, M. Dixon, L. K. Tyler, Cam-CAN, and R. N. Henson, The cambridge centre for ageing and neuroscience (Cam-CAN) data repository: Structural and functional mri, meg, and cognitive data from a cross-sectional adult lifespan sample, *NeuroImage* **144**, 262 (2017), data Sharing Part II.
- [40] G. Backus, A geometrical picture of anisotropic elastic tensors, *Reviews of Geophysics* **8**, 633 (1970).
- [41] J. Betten, Irreducible invariants of fourth-order tensors, *Mathematical Modelling* **8**, 29 (1987).
- [42] J. Betten, Invariants of fourth-order tensors, in *Applications of tensor functions in solid mechanics*, edited by J.-P. Boehler (Springer-Verlag, Vienna, Austria, 1987) Chap. 11, pp. 203–226.
- [43] A. Bóna, I. Bucataru, and M. Slawinski, Characterization of elasticity-tensor symmetries using  $su(2)$ , *Journal of Elasticity* **75**, 267 (2004).
- [44] M. Moakher, Fourth-order cartesian tensors: old and new facts, notions and applications, *The Quarterly Journal of Mechanics and Applied Mathematics* **61**, 181 (2008).
- [45] K. S. Thorne, Multipole expansions of gravitational radiation, *Rev. Mod. Phys.* **52**, 299 (1980).
- [46] M. Tinkham, *Group Theory and Quantum Mechanics (Dover Books on Chemistry)* (Dover Publications, 2003).
- [47] B. C. Hall, *Lie Groups, Lie Algebras, and Representations* (Springer, 2015).
- [48] S. Eriksson, S. Lasic, M. Nilsson, C.-F. Westin, and D. Topgaard, NMR diffusion-encoding with axial symmetry and variable anisotropy: Distinguishing between prolate and oblate microscopic diffusion tensors with unknown orientation distribution, *The Journal of Chemical Physics* **142**, 104201 (2015).
- [49] E. O. Stejskal and T. E. Tanner, Spin diffusion measurements: spin echoes in the presence of a time-dependent field gradient, *The Journal of Chemical Physics* **42**, 288 (1965).
- [50] H. Hopf, Über die Abbildungen der dreidimensionalen Sphäre auf die Kugelfläche, *Mathematische Annalen* **104** (1931).
- [51] S. Lasič, F. Szczepankiewicz, S. Eriksson, M. Nilsson, and D. Topgaard, Microanisotropy imaging: quantification of microscopic diffusion anisotropy and orientational order parameter by diffusion MRI with magic-angle spinning of the q-vector, *Frontiers in Physics* **2**, 11 (2014).
- [52] J. H. Jensen, J. A. Helpert, A. Ramani, H. Lu, and K. Kaczynski, Diffusional Kurtosis Imaging: The quantification of non-gaussian water diffusion by means of magnetic resonance imaging, *Magnetic Resonance in Medicine* **53**, 1432 (2005).
- [53] Y. Itin and F. W. Hehl, The constitutive tensor of linear elasticity: Its decompositions, cauchy relations, null lagrangians, and wave propagation, *Journal of Mathematical Physics* **54**, 042903 (2013).
- [54] Y. Itin and F. W. Hehl, Irreducible decompositions of the elasticity tensor under the linear and orthogonal groups and their physical consequences, in *Journal of Physics: Conference Series*, Vol. 597 (IOP Publishing, 2015) p. 012046.
- [55] A. Ghosh, T. Papadopoulo, and R. Deriche, Biomarkers for HARDI: 2nd & 4th order tensor invariants, in *2012 9th IEEE International Symposium on Biomedical Imaging (ISBI)* (2012) pp. 26–29.
- [56] P. J. Basser and S. Pajevic, Spectral decomposition of a 4th-order covariance tensor: Applications to diffusion tensor MRI, *Signal Processing* **87**, 220 (2007).
- [57] L. Qi, D. Han, and E. X. Wu, Principal invariants and inherent parameters of diffusion kurtosis tensors, *Journal of Mathematical Analysis and Applications* **349**, 165 (2009).
- [58] T. Papadopoulo, A. Ghosh, and R. Deriche, Complete set of invariants of a 4th order tensor: The 12 tasks of hardi from ternary quartics, in *Medical Image Computing and Computer-Assisted Intervention – MICCAI 2014* (Springer International Publishing, Cham, 2014) pp. 233–240.
- [59] H. Lu, J. Jensen, A. Ramani, and J. Helpert, Three-dimensional characterization of non-gaussian water diffusion in humans using diffusion kurtosis imaging, *NMR in Biomedicine* **19**, 236 (2006).
- [60] B. Hansen, T. E. Lund, R. Sangill, and S. N. Jespersen, Experimentally and computationally fast method for estimation of a mean kurtosis, *Magnetic Resonance in Medicine* **69**, 1754 (2013).
- [61] B. Hansen, N. Shemesh, and S. N. Jespersen, Fast imaging of mean, axial and radial diffusion kurtosis, *NeuroImage* **142**, 381 (2016).
- [62] B. Ades-Aron, S. Coelho, G. Lemberskiy, J. Veraart, S. Baete, T. M. Shepherd, D. S. Novikov, and E. Fieremans, [Denoising improves cross-scanner and cross-protocol test-retest reproducibility of higher-order diffusion metrics](#) (2024), [arXiv:2407.18253 \[physics.med-ph\]](#).
- [63] F. Szczepankiewicz, D. van Westen, E. Englund, C.-F. Westin, F. Ståhlberg, J. Lätt, P. C. Sundgren, and M. Nilsson, The link between diffusion MRI and tumor heterogeneity: Mapping cell eccentricity and density by diffusional variance decomposition (DIVIDE), *NeuroImage* **142**, 522 (2016).
- [64] R. N. Henriques, S. N. Jespersen, and N. Shemesh, Evidence for microscopic kurtosis in neural tissue revealed by correlation tensor mri, *Magnetic Resonance in Medicine* **86**, 3111 (2021).

- [65] R. N. Henriques, S. N. Jespersen, and N. Shemesh, Microscopic anisotropy misestimation in spherical-mean single diffusion encoding MRI, *Magnetic Resonance in Medicine* **81**, 3245 (2019).
- [66] G. R. Glenn, J. A. Helpert, A. Tabesh, and J. H. Jensen, Quantitative assessment of diffusional kurtosis anisotropy, *NMR in Biomedicine* **28**, 448 (2015).
- [67] E. S. Hui, M. M. Cheung, L. Qi, and E. X. Wu, Towards better mr characterization of neural tissues using directional diffusion kurtosis analysis, *NeuroImage* **42**, 122 (2008).
- [68] J. H. Jensen and J. A. Helpert, Mri quantification of non-gaussian water diffusion by kurtosis analysis, *NMR in Biomedicine* **23**, 698 (2010).
- [69] M. Nilsson, F. Szczepankiewicz, J. Brabec, M. Taylor, C.-F. Westin, A. Golby, D. van Westen, and P. C. Sundgren, Tensor-valued diffusion MRI in under 3 minutes: an initial survey of microscopic anisotropy and tissue heterogeneity in intracranial tumors, *Magnetic Resonance in Medicine* **83**, 608 (2020).
- [70] F. Szczepankiewicz, S. Hoge, and C.-F. Westin, Linear, planar and spherical tensor-valued diffusion mri data by free waveform encoding in healthy brain, water, oil and liquid crystals, *Data in Brief* **25**, 104208 (2019).
- [71] P. Seymour and T. Zaslavsky, Averaging sets: A generalization of mean values and spherical designs, *Advances in Mathematics* **52**, 213 (1984).
- [72] L. Ning, F. Szczepankiewicz, M. Nilsson, Y. Rathi, and C.-F. Westin, Probing tissue microstructure by diffusion skewness tensor imaging, *Scientific Reports* **135** (2021).
- [73] V. G. Kiselev and K. A. Il'yasov, Is the "biexponential diffusion" biexponential?, *Magnetic Resonance in Medicine* **57**, 464 (2007).
- [74] J. a. P. de Almeida Martins and D. Topgaard, Two-dimensional correlation of isotropic and directional diffusion using nmr, *Phys. Rev. Lett.* **116**, 087601 (2016).
- [75] K. N. Magdoom, S. Pajevic, G. Dario, and P. J. Basser, A new framework for mr diffusion tensor distribution, *Scientific Reports* **11**, 2766 (2021).
- [76] S. N. Jespersen, Equivalence of double and single wave vector diffusion contrast at low diffusion weighting, *NMR in Biomedicine* **25**, 813 (2011).
- [77] P. Basser and S. Pajevic, A normal distribution for tensor-valued random variables: applications to diffusion tensor MRI, *IEEE Transactions on Medical Imaging* **22**, 785 (2003).
- [78] B. Jian, B. C. Vemuri, E. Özarslan, P. R. Carney, and T. H. Mareci, A novel tensor distribution model for the diffusion-weighted mr signal, *NeuroImage* **37**, 164 (2007).
- [79] G. R. Glenn, J. A. Helpert, A. Tabesh, and J. H. Jensen, Quantitative assessment of diffusional kurtosis anisotropy, *NMR in Biomedicine* **28**, 448 (2015).
- [80] S. N. Jespersen, C. D. Kroenke, L. Ostergaard, J. J. H. Ackerman, and D. A. Yablonskiy, Modeling dendrite density from magnetic resonance diffusion measurements, *NeuroImage* **34**, 1473 (2007).
- [81] S. N. Jespersen, C. R. Bjarkam, J. R. Nyengaard, M. M. Chakravarty, B. Hansen, T. Vosegaard, L. Ostergaard, D. Yablonskiy, N. C. Nielsen, and P. Vestergaard-Poulsen, Neurite density from magnetic resonance diffusion measurements at ultrahigh field: Comparison with light microscopy and electron microscopy, *NeuroImage* **49**, 205 (2010).
- [82] E. Fieremans, J. H. Jensen, and J. A. Helpert, White matter characterization with diffusional kurtosis imaging, *NeuroImage* **58**, 177 (2011).
- [83] H. Zhang, T. Schneider, C. A. Wheeler-Kingshott, and D. C. Alexander, NODDI: Practical in vivo neurite orientation dispersion and density imaging of the human brain, *NeuroImage* **61**, 1000 (2012).
- [84] S. N. Sotiropoulos, T. E. Behrens, and S. Jbabdi, Ball and rackets: Inferring fiber fanning from diffusion-weighted MRI, *NeuroImage* **60**, 1412 (2012).
- [85] J. H. Jensen, G. Russell Glenn, and J. A. Helpert, Fiber ball imaging, *NeuroImage* **124**, 824 (2016).
- [86] G. Racah, Theory of complex spectra. ii, *Phys. Rev.* **62**, 438 (1942).
- [87] E. U. Condon and G. H. Shortley, *The theory of atomic spectra* (The Cambridge University Press., Cambridge, 1964.).
- [88] J. M. Pozo, S. Coelho, and A. F. Frangi, Tensorial formulation allowing to verify or falsify the microstructural standard model from multidimensional diffusion MRI, in *Proceedings of the International Society of Magnetic Resonance in Medicine*, Vol. 3560 (Wiley, 2019).
- [89] F. Szczepankiewicz, C.-F. Westin, and M. Nilsson, Maxwell-compensated design of asymmetric gradient waveforms for tensor-valued diffusion encoding, *Magnetic Resonance in Medicine* **82**, 1424 (2019).
- [90] F. Szczepankiewicz, J. Sjölund, F. Ståhlberg, J. Lätt, and M. Nilsson, Tensor-valued diffusion encoding for diffusional variance decomposition (divide): Technical feasibility in clinical mri systems, *PLOS ONE* **14**, 1 (2019).
- [91] G. Lemberskiy, S. Baete, J. Veraart, T. Shepherd, E. Fieremans, and D. S. Novikov, Achieving sub-mm clinical diffusion MRI resolution by removing noise during reconstruction using random matrix theory, In *Proceedings 27th Scientific Meeting, 0770, International Society for Magnetic Resonance in Medicine, Montreal, Canada, 2019* (2019).
- [92] J. Veraart, E. Fieremans, and D. S. Novikov, Diffusion MRI noise mapping using random matrix theory, *Magnetic Resonance in Medicine* **76**, 1582 (2016).
- [93] T. Chen, P. B. Catrysse, A. E. Gamal, and B. A. Wandell, How small should pixel size be?, in *Proceedings of SPIE*, Vol. 3965 (2000) pp. 451–459.
- [94] H.-H. Lee, D. S. Novikov, and E. Fieremans, Removal of partial fourier-induced gibbs (rpg) ringing artifacts in MRI, *Magnetic Resonance in Medicine* **86**, 2733 (2021).
- [95] S. M. Smith, M. Jenkinson, M. W. Woolrich, C. F. Beckmann, T. E. J. Behrens, H. Johansen-Berg, P. Bannister, M. Luca, I. Drobnjak, D. Flitney, R. Niazy, J. Saunders, J. Vickers, Y. Zhang, N. De Stefano, M. Brady, and P. Matthews, Advances in functional and structural mr image analysis and implementation as fsl, *NeuroImage* **23 Suppl 1**, S208 (2004).
- [96] J. L. Andersson, S. Skare, and J. Ashburner, How to correct susceptibility distortions in spin-echo echo-planar images: application to diffusion tensor imaging, *NeuroImage* **20**, 870 (2003).
- [97] N. Wiest-Daesslé, S. Prima, P. Coupé, S. P. Morrissey, and C. Barillot, Non-local means variants for denoising of diffusion-weighted and diffusion tensor MRI, in *Medical Image Computing and Computer-Assisted Intervention (MICCAI)*, Vol. 10 (Springer, 2007) pp. 344–351.
- [98] J. Veraart, J. Sijbers, S. Sunaert, A. Leemans, and B. Jeurissen, Weighted linear least squares estimation of diffusion MRI parameters: Strengths, limitations, and pitfalls, *NeuroImage* **81**, 335 (2013).
- [99] M. Herberthson, D. Boito, T. D. Haije, A. Feragen, C.-F. Westin, and E. Özarslan, Q-space trajectory imaging with positivity constraints (QTI+), *NeuroImage* **238**, 118198 (2021).
- [100] Particle Data Group, Review of Particle Physics, *Progress of Theoretical and Experimental Physics* **2022**, 083C01 (2022).

SUPPLEMENTARY INFORMATION — *GEOMETRY OF THE CUMULANT SERIES IN NEUROIMAGING*

Santiago Coelho, Filip Szczepankiewicz, Els Fieremans, and Dmitry S. Novikov

Corresponding authors: Santiago.Coelho@nyulangone.org (SC) and Dmitry.Novikov@nyulangone.org (DSN)

**S1. IRREDUCIBLE DECOMPOSITION INTO A SUM OF TENSORS WITH THE SAME ORDER, EQS. (45)–(49)**

To find all the spherical tensor components (50) of the decomposition (45) used in this work we need to project on the generalized basis (46). The normalization coefficients (48) can be found straightforwardly:

$$\begin{aligned}
 \mathcal{Y}_{ij}^{00} &= \delta_{ij}, \quad \zeta(2, 0) = \mathcal{Y}_{ij}^{00} \mathcal{Y}_{ij}^{00} = \delta_{ij} \delta_{ij} = 3; \\
 \mathcal{Y}_{ijkl}^{00} &= \delta_{(ij)\delta_{kl}}, \quad \zeta(4, 0) = \mathcal{Y}_{ijkl}^{00} \delta_{ij} \delta_{kl} = \frac{1}{3} (\delta_{ij} \delta_{kl} + \delta_{ik} \delta_{jl} + \delta_{il} \delta_{jk}) \delta_{ij} \delta_{kl} = \frac{1}{3} (3 \cdot 3 + 3 + 3) = 5; \\
 \mathcal{Y}_{ijkl}^{2m} \delta_{kl} &= \mathcal{Y}_{(ij}^{2m} \delta_{kl)} \delta_{kl} = \frac{1}{6} (\mathcal{Y}_{ij}^{2m} \delta_{kl} + \mathcal{Y}_{il}^{2m} \delta_{jk} + \mathcal{Y}_{ik}^{2m} \delta_{lj} + \mathcal{Y}_{kl}^{2m} \delta_{ij} + \mathcal{Y}_{jk}^{2m} \delta_{il} + \mathcal{Y}_{lj}^{2m} \delta_{ik}) \delta_{kl} = \frac{7}{6} \mathcal{Y}_{ij}^{2m}; \\
 \mathcal{Y}_{ijkl}^{2m} \mathcal{Y}_{ijkl}^{2m'} &= \mathcal{Y}_{(ij}^{2m} \delta_{kl)} \delta_{kl} \mathcal{Y}_{ij}^{2m'} = \frac{7}{6} \mathcal{Y}_{ij}^{2m} \mathcal{Y}_{ij}^{2m'} = \frac{7}{6} \cdot \frac{3}{2} \delta_{mm'} \equiv \zeta(4, 2) \delta_{mm'}, \quad \zeta(4, 2) = \frac{7}{4}.
 \end{aligned} \tag{S1}$$

In the last equation we used the normalization  $\zeta(\ell, \ell)$  (43) for  $\ell = 2$ .

For completeness, in the remainder of this Section we motivate a general normalization formula (48) for all  $L$  and  $\ell$ . Equation (48) relies on the following identity to be derived below:

$$\mathcal{Y}_{i_1 \dots i_L}^{\ell m} \delta_{i_{L-1} i_L} = \frac{(L + \ell + 1)(L - \ell)}{L(L - 1)} \mathcal{Y}_{i_1 \dots i_{L-2}}^{\ell m} \quad \text{for } L \geq \ell + 2; \quad \text{and } 0 \quad \text{for } L = \ell. \tag{S2}$$

Assuming Eq. (S2) holds, we apply it recursively

$$\mathcal{Y}_{i_1 \dots i_L}^{\ell m} \delta_{i_{\ell+1} i_{\ell+2}} \dots \delta_{i_{L-1} i_L} = \frac{(L + \ell + 1)(L + \ell - 1) \dots (2\ell + 3)(L - \ell)(L - \ell - 2) \dots 2}{L(L - 1)(L - 2) \dots (\ell + 1)} \mathcal{Y}_{i_1 \dots i_\ell}^{\ell m}. \tag{S3}$$

Combining Eqs. (S3) and (43) allows us to obtain Eq. (48):

$$\zeta(L, \ell) = \mathcal{Y}_{i_1 \dots i_L}^{\ell m} \mathcal{Y}_{i_1 \dots i_\ell}^{\ell m} \delta_{i_{\ell+1} i_{\ell+2}} \dots \delta_{i_{L-1} i_L} = \frac{(L + \ell + 1)!!(L - \ell)!!}{L!(2\ell + 1)}.$$

To derive Eq. (S2), consider as an example the case for  $L = \ell + 2$ :

$$\begin{aligned}
 \mathcal{Y}_{i_1 \dots i_L}^{\ell m} \delta_{i_{L-1} i_L} &= \mathcal{Y}_{(i_1 \dots i_\ell}^{\ell m} \delta_{i_{L-1} i_L)} \delta_{i_{L-1} i_L} \\
 &= \frac{\ell! 2!}{(\ell + 2)!} \left( \mathcal{Y}_{i_1 \dots i_\ell}^{\ell m} \delta_{i_{L-1} i_L} + \mathcal{Y}_{i_{L-1} i_2 \dots i_\ell}^{\ell m} \delta_{i_1 i_L} + \mathcal{Y}_{i_1 i_{L-1} i_3 \dots i_\ell}^{\ell m} \delta_{i_2 i_L} + \dots + \mathcal{Y}_{i_1 \dots i_{\ell-1} i_{L-1}}^{\ell m} \delta_{i_\ell i_L} \right. \\
 &\quad + \mathcal{Y}_{i_L i_2 \dots i_\ell}^{\ell m} \delta_{i_{L-1} i_1} + \mathcal{Y}_{i_1 i_L i_3 \dots i_\ell}^{\ell m} \delta_{i_{L-1} i_2} + \dots + \mathcal{Y}_{i_1 \dots i_{\ell-1} i_L}^{\ell m} \delta_{i_{L-1} i_\ell} \\
 &\quad \left. + \mathcal{Y}_{i_{L-1} i_L i_3 \dots i_\ell}^{\ell m} \delta_{i_1 i_2} + \mathcal{Y}_{i_{L-1} i_2 i_L i_4 \dots i_\ell}^{\ell m} \delta_{i_1 i_3} + \dots + \mathcal{Y}_{i_1 \dots i_{\ell-2} i_{L-1} i_L}^{\ell m} \delta_{i_{\ell-1} i_\ell} \right) \delta_{i_{L-1} i_L} \\
 &= \frac{\ell! 2!}{(\ell + 2)!} \left( 3 \mathcal{Y}_{i_1 \dots i_\ell}^{\ell m} + 2\ell \mathcal{Y}_{i_1 \dots i_\ell}^{\ell m} + \binom{\ell}{2} \times 0 \right) = \frac{2(2\ell + 3)}{(\ell + 1)(\ell + 2)} \mathcal{Y}_{i_1 \dots i_\ell}^{\ell m},
 \end{aligned} \tag{S4}$$

which can be generalized for arbitrary  $L > \ell$  to derive Eq. (S2). The rationale behind the derivation in Eq. (S4) is that one must expand the symmetrized  $\mathcal{Y}_{i_1 \dots i_L}^{\ell m}$  into a sum of all permutations of subindices where  $i_{L-1}, i_L$  are either part of  $\mathcal{Y}^{\ell m}$  or part of a product of  $(L - \ell)/2$  Kronecker deltas (in this case, a single one). Then, we have to contract indices  $i_{L-1}, i_L$  on each term and add the contributions. Contracting any two indices of  $\mathcal{Y}_{i_1 \dots i_\ell}^{\ell m}$  yields 0 due to STF property, while all combinations of contractions of the products of the Kronecker symbols can be computed using

$$\delta_{(i_1 i_2} \dots \delta_{i_{L-1} i_L)} \delta_{(i_{\ell+1} i_{\ell+2}} \dots \delta_{i_{L-1} i_L)} = \frac{L + 1}{\ell + 1} \delta_{(i_1 i_2} \dots \delta_{i_{L-3} i_{L-2}}). \tag{S5}$$

**S2. IRREDUCIBLE DECOMPOSITION OF SPHERICAL TENSOR PRODUCTS**

**A. Clebsch-Gordan coefficients and products of spherical harmonics**

As the relation between the  $\mathbb{C}$  tensor and the covariances of compartment diffusion tensors maps onto the addition of angular momenta, we remind that from the representation theory standpoint, the addition of angular momenta  $\vec{\ell}_1$  and  $\vec{\ell}_2$  corresponds

to the tensor product of two irreducible representations of  $\text{SO}(3)$  with dimensions  $2\ell_1 + 1$  and  $2\ell_2 + 1$ . This tensor product of dimension  $(2\ell_1 + 1)(2\ell_2 + 1)$  is reducible, and splits into a sum of irreducible representations with  $L = |\ell_1 - \ell_2|, \dots, \ell_1 + \ell_2$ , each one entering exactly once [46, 47]. The orthonormal basis elements

$$|LM\rangle = \sum_{m_1+m_2=M} |\ell_1 m_1 \ell_2 m_2\rangle \langle \ell_1 m_1 \ell_2 m_2 | LM \rangle, \quad M = -L \dots L \quad (\text{S6})$$

of each such irreducible representation labeled by  $L$ , are expanded in terms of the basis elements of  $|\ell_1 m_1 \ell_2 m_2\rangle = |\ell_1 m_1\rangle \otimes |\ell_2 m_2\rangle$  of the tensor product, where  $m_1 = -\ell_1 \dots \ell_1$ ,  $m_2 = -\ell_2 \dots \ell_2$ , and  $\langle \ell_1 m_1 \ell_2 m_2 | LM \rangle$  are the Clebsch–Gordan coefficients.

In this Section, we will use the complex spherical harmonics and tensors. We also adopt the Condon-Shortley convention [87] for the complex spherical harmonics and tensors [45], for which the Clebsch-Gordan coefficients are purely real. In the Racah normalization (41), the SH  $Y^{\ell m}(\hat{\mathbf{n}}) = \mathcal{D}_{m0}^{\ell*}(\hat{\mathbf{n}})$  are given by the matrix elements of the Wigner rotation matrices  $\mathcal{D}_{mm'}^{\ell}$  parametrized by the two Euler angles that are the polar and azimuthal angles of  $\hat{\mathbf{n}}$ , and are independent of the third Euler angle for  $m' = 0$ . Taking the  $\langle \ell_1 m_1 \ell_2 m_2 | \dots | \ell_1 0 \ell_2 0 \rangle$  matrix element of the tensor product  $\mathcal{D}^{\ell_1} \otimes \mathcal{D}^{\ell_2} = \oplus_{L=|\ell_1-\ell_2|^{\ell_1+\ell_2}} \mathcal{D}^L$ ,

$$Y^{\ell_1 m_1}(\hat{\mathbf{n}}) Y^{\ell_2 m_2}(\hat{\mathbf{n}}) = \sum_{L,M} \langle \ell_1 0 \ell_2 0 | L 0 \rangle \langle \ell_1 m_1 \ell_2 m_2 | LM \rangle Y^{LM}(\hat{\mathbf{n}}), \quad (\text{S7})$$

one obtains the well-known SH identity in Racah normalization (assuming the normalized measure  $\int_{\mathbb{S}^2} d\hat{\mathbf{n}} = \int d\Omega_{\hat{\mathbf{n}}}/4\pi \equiv 1$ )

$$\int_{\mathbb{S}^2} d\hat{\mathbf{n}} Y^{\ell_1 m_1}(\hat{\mathbf{n}}) Y^{\ell_2 m_2}(\hat{\mathbf{n}}) Y^{LM*}(\hat{\mathbf{n}}) = \frac{1}{2L+1} \langle \ell_1 0 \ell_2 0 | L 0 \rangle \langle \ell_1 m_1 \ell_2 m_2 | LM \rangle. \quad (\text{S8})$$

### B. Derivation of Eq. (53)

The derivation will be based on the analog of Eq. (S8) for the basis STF tensors, with the orthogonality over the unit sphere substituted by taking full trace. For that, we make use of the fully symmetric product of Kronecker symbols  $I_{i_1 \dots i_\ell}$  and Eq. (2.3) from Thorne [45]:

$$I_{i_1 \dots i_\ell} \equiv \delta_{(i_1 i_2 \dots i_{\ell-1} i_\ell)} = (\ell + 1) \int_{\mathbb{S}^2} d\hat{\mathbf{n}} n_{i_1} \dots n_{i_\ell}, \quad d\hat{\mathbf{n}} \equiv \frac{d\Omega_{\hat{\mathbf{n}}}}{4\pi}. \quad (\text{S9})$$

A useful relation then comes from combining the orthogonality (41) of spherical harmonics, and Eq. (S9):

$$\mathcal{Y}_{i_1 \dots i_\ell}^{\ell m*} \mathcal{Y}_{j_1 \dots j_{\ell'}}^{\ell' m'} I_{i_1 \dots i_\ell j_1 \dots j_{\ell'}} = \delta_{\ell \ell'} \delta_{mm'}, \quad (\text{S10})$$

which can be extended to a more general scenario applying Eq. (47):

$$\mathcal{Y}_{i_1 \dots i_L}^{\ell m*} \mathcal{Y}_{j_1 \dots j_{L'}}^{\ell' m'} I_{i_1 \dots i_L j_1 \dots j_{L'}} = \frac{L + L' + 1}{2\ell + 1} \delta_{\ell \ell'} \delta_{mm'} \quad \text{for the case where } L \geq \ell, L' \geq \ell'. \quad (\text{S11})$$

Likewise, we now can rewrite Eq. (S8) by replacing the integrals over  $n_{i_1} n_{i_2} \dots n_{i_k}$  with Eq. (S9):

$$\mathcal{Y}_{(i_1 \dots i_{\ell_1}}^{\ell_1 m_1} \mathcal{Y}_{j_1 \dots j_{\ell_2})}^{\ell_2 m_2} \mathcal{Y}_{k_1 \dots k_{\ell_1 + \ell_2}}^{LM*} I_{i_1 \dots i_{\ell_1} j_1 \dots j_{\ell_2} k_1 \dots k_{\ell_1 + \ell_2}} = \frac{2\ell_1 + 2\ell_2 + 1}{2L + 1} \langle \ell_1 0 \ell_2 0 | L 0 \rangle \langle \ell_1 m_1 \ell_2 m_2 | LM \rangle. \quad (\text{S12})$$

The term  $\mathcal{Y}_{(i_1 \dots i_{\ell_1}}^{\ell_1 m_1} \mathcal{Y}_{j_1 \dots j_{\ell_2})}^{\ell_2 m_2}$  is a symmetric tensor of order  $\ell_1 + \ell_2$ . Thus, we can expand it as a linear combination of basis tensors  $\mathcal{Y}_{i_1 \dots i_{\ell_1} j_1 \dots j_{\ell_2}}^{\ell' m'}$ , Eq. (46), with degrees  $\ell' = 0, 2, \dots, \ell_1 + \ell_2$ . When computing the tensor products on the left side of Eq. (S12), only the basis term  $\ell' = L$  of the expansion of  $\mathcal{Y}_{(i_1 \dots i_{\ell_1}}^{\ell_1 m_1} \mathcal{Y}_{j_1 \dots j_{\ell_2})}^{\ell_2 m_2}$  returns a nonzero value. If we call  $\xi$  the coefficient accompanying the  $\ell' = L$  term of the expansion, then Eq. (S12) can be written as

$$\mathcal{Y}_{(i_1 \dots i_{\ell_1}}^{\ell_1 m_1} \mathcal{Y}_{j_1 \dots j_{\ell_2})}^{\ell_2 m_2} \mathcal{Y}_{k_1 \dots k_{\ell_1 + \ell_2}}^{LM*} I_{i_1 \dots i_{\ell_1} j_1 \dots j_{\ell_2} k_1 \dots k_{\ell_1 + \ell_2}} = \xi \mathcal{Y}_{i_1 \dots i_{\ell_1} j_1 \dots j_{\ell_2}}^{LM} \mathcal{Y}_{k_1 \dots k_{\ell_1 + \ell_2}}^{LM*} I_{i_1 \dots i_{\ell_1} j_1 \dots j_{\ell_2} k_1 \dots k_{\ell_1 + \ell_2}}, \quad (\text{S13})$$

which combined with Eq. (S11) provides the value  $\xi = \langle \ell_1 0 \ell_2 0 | L 0 \rangle \langle \ell_1 m_1 \ell_2 m_2 | LM \rangle$ . Using Eq. (48), we can write the product

$$\mathcal{Y}_{(i_1 \dots i_{\ell_1}}^{\ell_1 m_1} \mathcal{Y}_{j_1 \dots j_{\ell_2})}^{\ell_2 m_2} \mathcal{Y}_{i_1 \dots i_{\ell_1} j_1 \dots j_{\ell_2}}^{LM*} = \xi \cdot \zeta(\ell_1 + \ell_2, L) = \zeta(\ell_1 + \ell_2, L) \langle \ell_1 0 \ell_2 0 | L 0 \rangle \langle \ell_1 m_1 \ell_2 m_2 | LM \rangle, \quad \ell_1 + \ell_2 \geq L, \quad (\text{S14})$$

since only the basis term  $\ell' = L$  of the expansion of  $\mathcal{Y}_{(i_1 \dots i_{\ell_1}}^{\ell_1 m_1} \mathcal{Y}_{j_1 \dots j_{\ell_2})}^{\ell_2 m_2}$  returns a nonzero value, and  $\zeta(\ell_1 + \ell_2, L)$  is the projection of the basis tensor onto itself, Eq. (48). Substituting  $\ell_1 = \ell_2 = 2$  in Eq. (S14) yields Eq. (53).

### C. Relation between Q and T tensors and compartmental spherical tensor covariances

Clebsch–Gordan coefficients are sparse since only those satisfying  $m_1 + m_2 = M$  are nonzero (19 out of 125 for  $\ell_1 = \ell_2 = L = 2$  and 25 out of 225 for  $\ell_1 = \ell_2 = 2, L = 4$ ). We can substitute these in Eq. (8b), or equivalently Eq. (54), and combine it with Eq. (8a) to get the system:

$$\begin{aligned}
Q^{00} &= \langle\langle (D^{00})^2 \rangle\rangle, \\
Q^{2m} &= 2 \langle\langle D^{00} D^{2m} \rangle\rangle \quad \text{for } m = -2, -1, \dots, 2; \\
T^{00} &= \frac{1}{\sqrt{5}} \left( 2 \frac{1}{\sqrt{5}} \langle\langle D^{2-2} D^{22} \rangle\rangle - 2 \frac{1}{\sqrt{5}} \langle\langle D^{2-1} D^{21} \rangle\rangle + \frac{1}{\sqrt{5}} \langle\langle (D^{20})^2 \rangle\rangle \right), \\
T^{2-2} &= -\sqrt{\frac{2}{7}} \left( 2 \sqrt{\frac{2}{7}} \langle\langle D^{2-2} D^{20} \rangle\rangle - \sqrt{\frac{3}{7}} \langle\langle (D^{2-1})^2 \rangle\rangle \right), \\
T^{2-1} &= -\sqrt{\frac{2}{7}} \left( 2 \sqrt{\frac{3}{7}} \langle\langle D^{2-2} D^{21} \rangle\rangle - 2 \sqrt{\frac{1}{14}} \langle\langle D^{2-1} D^{20} \rangle\rangle \right), \\
T^{20} &= -\sqrt{\frac{2}{7}} \left( 2 \sqrt{\frac{2}{7}} \langle\langle D^{2-2} D^{22} \rangle\rangle + 2 \sqrt{\frac{1}{14}} \langle\langle D^{2-1} D^{21} \rangle\rangle - \sqrt{\frac{2}{7}} \langle\langle (D^{20})^2 \rangle\rangle \right), \\
T^{21} &= -\sqrt{\frac{2}{7}} \left( 2 \sqrt{\frac{3}{7}} \langle\langle D^{2-1} D^{22} \rangle\rangle - 2 \sqrt{\frac{1}{14}} \langle\langle D^{20} D^{21} \rangle\rangle \right), \\
T^{22} &= -\sqrt{\frac{2}{7}} \left( 2 \sqrt{\frac{2}{7}} \langle\langle D^{20} D^{22} \rangle\rangle - \sqrt{\frac{3}{7}} \langle\langle (D^{21})^2 \rangle\rangle \right), \\
T^{4-4} &= \sqrt{\frac{18}{35}} \langle\langle (D^{2-2})^2 \rangle\rangle, \\
T^{4-3} &= \sqrt{\frac{18}{35}} 2 \frac{1}{\sqrt{2}} \langle\langle D^{2-2} D^{2-1} \rangle\rangle, \\
T^{4-2} &= \sqrt{\frac{18}{35}} \left( 2 \sqrt{\frac{3}{14}} \langle\langle D^{2-2} D^{20} \rangle\rangle + \sqrt{\frac{4}{7}} \langle\langle (D^{2-1})^2 \rangle\rangle \right), \\
T^{4-1} &= \sqrt{\frac{18}{35}} \left( 2 \sqrt{\frac{1}{14}} \langle\langle D^{2-2} D^{21} \rangle\rangle + 2 \sqrt{\frac{3}{7}} \langle\langle D^{2-1} D^{20} \rangle\rangle \right), \\
T^{40} &= \sqrt{\frac{18}{35}} \left( 2 \sqrt{\frac{1}{70}} \langle\langle D^{2-2} D^{22} \rangle\rangle + 2 \sqrt{\frac{8}{35}} \langle\langle D^{2-1} D^{21} \rangle\rangle + \sqrt{\frac{18}{35}} \langle\langle (D^{20})^2 \rangle\rangle \right), \\
T^{41} &= \sqrt{\frac{18}{35}} \left( 2 \sqrt{\frac{1}{14}} \langle\langle D^{2-1} D^{22} \rangle\rangle + 2 \sqrt{\frac{3}{7}} \langle\langle D^{20} D^{21} \rangle\rangle \right), \\
T^{42} &= \sqrt{\frac{18}{35}} \left( 2 \sqrt{\frac{3}{14}} \langle\langle D^{20} D^{22} \rangle\rangle + \sqrt{\frac{4}{7}} \langle\langle (D^{21})^2 \rangle\rangle \right), \\
T^{43} &= \sqrt{\frac{18}{35}} 2 \frac{1}{\sqrt{2}} \langle\langle D^{21} D^{22} \rangle\rangle, \\
T^{44} &= \sqrt{\frac{18}{35}} \langle\langle (D^{22})^2 \rangle\rangle,
\end{aligned} \tag{S15}$$

where Clebsch–Gordan coefficients are written explicitly for the reader (see page 737 in Ref. [100] for a complete table). This shows how all covariances contribute to T and Q irreducible components. Solving for all the covariances gives

$$\begin{aligned}
\langle\langle (D^{00})^2 \rangle\rangle &= Q^{00}, & \langle\langle D^{00} D^{2m} \rangle\rangle &= \frac{1}{2} Q^{2m} \quad \text{for } m = -2, \dots, 2; \\
\langle\langle (D^{2-2})^2 \rangle\rangle &= \frac{\sqrt{70}}{6} T^{4-4}, & \langle\langle D^{2-2} D^{2-1} \rangle\rangle &= \frac{\sqrt{35}}{6} T^{4-3}, \\
\langle\langle D^{2-2} D^{20} \rangle\rangle &= \frac{\sqrt{15}}{6} T^{4-2} - T^{2-2}, & \langle\langle D^{2-2} D^{21} \rangle\rangle &= \frac{\sqrt{5}}{6} T^{4-1} - \frac{\sqrt{6}}{2} T^{2-1}, \\
\langle\langle D^{2-2} D^{22} \rangle\rangle &= \frac{1}{6} T^{40} - T^{20} + T^{00}, & \langle\langle (D^{2-1})^2 \rangle\rangle &= \frac{\sqrt{10}}{3} T^{4-2} + \frac{\sqrt{150}}{10} T^{2-2}, \\
\langle\langle D^{2-1} D^{20} \rangle\rangle &= \frac{\sqrt{30}}{6} T^{4-1} + \frac{1}{2} T^{2-1}, & \langle\langle D^{2-1} D^{21} \rangle\rangle &= \frac{2}{3} T^{40} - \frac{1}{2} T^{20} - T^{00}, \\
\langle\langle D^{2-1} D^{22} \rangle\rangle &= \frac{\sqrt{5}}{6} T^{41} - \frac{\sqrt{6}}{2} T^{21}, & \langle\langle (D^{20})^2 \rangle\rangle &= T^{40} + T^{20} + T^{00}, \\
\langle\langle D^{20} D^{21} \rangle\rangle &= \frac{\sqrt{30}}{6} T^{41} + \frac{1}{2} T^{21}, & \langle\langle D^{20} D^{22} \rangle\rangle &= \frac{\sqrt{15}}{6} T^{42} - T^{22}, \\
\langle\langle (D^{21})^2 \rangle\rangle &= \frac{\sqrt{10}}{3} T^{42} + \frac{\sqrt{150}}{10} T^{22}, & \langle\langle D^{21} D^{22} \rangle\rangle &= \frac{\sqrt{35}}{6} T^{43}, \\
\langle\langle (D^{22})^2 \rangle\rangle &= \frac{\sqrt{70}}{6} T^{44}.
\end{aligned} \tag{S16}$$

The sparsity of the QT decomposition is seen in all covariances depending on few T and Q elements. The simplicity of Eq. (S16) relies on the usage of the canonical, complex-valued spherical tensor basis. As the C tensor is real-valued, we can go back and

forth from complex to real spherical tensor representations. Specifically, to obtain real-SH covariances  $\langle\langle D^{\ell m} D^{\ell' m'} \rangle\rangle$ , one can take  $T^{\ell m}$  and  $Q^{\ell m}$  in the complex spherical tensor basis, compute  $\langle\langle D^{\ell m} D^{\ell' m'} \rangle\rangle$  using Eqs. (S16), and then convert the latter to the real spherical tensor basis, as spelled out in the following Supplementary Section S3.

### S3. RELATIONS BETWEEN REAL AND COMPLEX SPHERICAL TENSORS/HARMONICS

Since  $C$  is real-valued one may want to work with the real spherical tensor basis and, thus, write the solution (S16) for it. This is cumbersome because in the real basis Eq. (53) includes multiple combinations of Clebsch-Gordan coefficients  $\langle 2 \pm m_1 2 \pm m_2 | 2 \pm M \rangle$ . An alternative is to compute complex-valued  $\langle\langle D^{\ell m} D^{\ell' m'} \rangle\rangle$  using Eq. (S16) and then transform these to real-valued ones. This can be done using the relation between complex and real spherical basis tensors:

$$\mathcal{Y}_C^{\ell m} = \begin{cases} \frac{1}{\sqrt{2}} (\mathcal{Y}_R^{\ell-m} - i \mathcal{Y}_R^{\ell m}) & \text{if } m < 0 \\ \mathcal{Y}_R^{\ell 0} & \text{if } m = 0 \\ \frac{(-1)^m}{\sqrt{2}} (\mathcal{Y}_R^{\ell m} + i \mathcal{Y}_R^{\ell-m}) & \text{if } m > 0 \end{cases}, \quad \mathcal{Y}_R^{\ell m} = \begin{cases} (-1)^m \sqrt{2} \text{Im}(\mathcal{Y}_C^{\ell-m}) & \text{if } m < 0 \\ \mathcal{Y}_C^{\ell 0} & \text{if } m = 0 \\ (-1)^m \sqrt{2} \text{Re}(\mathcal{Y}_C^{\ell m}) & \text{if } m > 0 \end{cases}, \quad (\text{S17})$$

where  $\mathcal{Y}_C^{\ell m}$  and  $\mathcal{Y}_R^{\ell m}$  are the complex and real STF basis tensors (identical relations apply to the SH basis). Note that, unlike the complex spherical tensors, the real spherical tensor basis (following conventions) does *not* include the Condon-Shortley phase. Since compartmental diffusion tensors  $D_{ij}$  are real-valued, we can map complex-valued  $D^{\ell m}$  into real-valued ones using the following relations:

$$D_R^{\ell m} = \begin{cases} (-1)^{m+1} \sqrt{2} \text{Im}(D_C^{\ell-m}) & \text{if } m < 0 \\ D_C^{\ell 0} & \text{if } m = 0 \\ (-1)^m \sqrt{2} \text{Re}(D_C^{\ell m}) & \text{if } m > 0 \end{cases}, \quad \text{and} \quad D_C^{\ell m*} = (-1)^m D_C^{\ell-m}, \quad (\text{S18})$$

where  $D_R^{\ell m}$  and  $D_C^{\ell m}$  are spherical tensor coefficients using either real or complex basis. Thus, the mapping  $\langle\langle D_C^{\ell m} D_C^{\ell' m'} \rangle\rangle \rightarrow \langle\langle D_R^{\ell m} D_R^{\ell' m'} \rangle\rangle$  becomes:

$$\langle\langle D_R^{\ell m} D_R^{\ell' m'} \rangle\rangle = \begin{cases} \langle\langle D_C^{00} D_C^{00} \rangle\rangle & \text{if } \ell = 0, m = 0, \ell' = 0, m' = 0, \\ \sqrt{2} \text{Im} \left( \langle\langle D_C^{00} D_C^{2m'} \rangle\rangle \right) & \text{if } \ell = 0, m = 0, \ell' = 2, m' < 0, \\ \langle\langle D_C^{00} D_C^{20} \rangle\rangle & \text{if } \ell = 0, m = 0, \ell' = 2, m' = 0, \\ (-1)^{m'} \sqrt{2} \text{Re} \left( \langle\langle D_C^{00} D_C^{2m'} \rangle\rangle \right) & \text{if } \ell = 0, m = 0, \ell' = 2, m' > 0, \\ -\text{Re} \left( \langle\langle D_C^{2m} D_C^{2m'} \rangle\rangle \right) + (-1)^{m'} \text{Re} \left( \langle\langle D_C^{2m} D_C^{2-m'} \rangle\rangle \right) & \text{if } \ell = 2, m < 0, \ell' = 2, m' < 0, \\ \sqrt{2} \text{Im} \left( \langle\langle D_C^c D_C^c \rangle\rangle \right) & \text{if } \ell = 2, m < 0, \ell' = 2, m' = 0, \\ (-1)^{m'} \text{Im} \left( \langle\langle D_C^{2m} D_C^{2m'} \rangle\rangle \right) + \text{Im} \left( \langle\langle D_C^{2m} D_C^{2-m'} \rangle\rangle \right) & \text{if } \ell = 2, m < 0, \ell' = 2, m' > 0, \\ \langle\langle D_C^{20} D_C^{20} \rangle\rangle & \text{if } \ell = 2, m = 0, \ell' = 2, m' = 0, \\ (-1)^{m'} \sqrt{2} \text{Re} \left( \langle\langle D_C^{20} D_C^{2m'} \rangle\rangle \right) & \text{if } \ell = 2, m = 0, \ell' = 2, m' > 0, \\ (-1)^{m+m'} \text{Re} \left( \langle\langle D_C^{2m} D_C^{2m'} \rangle\rangle \right) + (-1)^m \text{Re} \left( \langle\langle D_C^{2m} D_C^{2-m'} \rangle\rangle \right) & \text{if } \ell = 2, m > 0, \ell' = 2, m' > 0. \end{cases} \quad (\text{S19})$$

### S4. SECOND-ORDER 6D REPRESENTATION FOR FULLY SYMMETRIC FOURTH-ORDER 3D TENSORS

$$\mathbf{S}_{6 \times 6}^{(4)} = \begin{pmatrix} \frac{\sqrt{35}}{8} \mathbf{S}^{44} - \frac{\sqrt{5}}{4} \mathbf{S}^{42} + \frac{3}{8} \mathbf{S}^{40} & -\frac{\sqrt{35}}{8} \mathbf{S}^{44} + \frac{1}{8} \mathbf{S}^{40} & \frac{\sqrt{5}}{4} \mathbf{S}^{42} - \frac{1}{2} \mathbf{S}^{40} & \frac{\sqrt{70}}{8} \mathbf{S}^{4-4} - \frac{\sqrt{10}}{8} \mathbf{S}^{4-2} & \frac{\sqrt{35}}{8} \mathbf{S}^{43} - \frac{3\sqrt{5}}{8} \mathbf{S}^{41} & \frac{\sqrt{35}}{8} \mathbf{S}^{4-3} - \frac{\sqrt{5}}{8} \mathbf{S}^{4-1} \\ -\frac{\sqrt{35}}{8} \mathbf{S}^{44} + \frac{1}{8} \mathbf{S}^{40} & \frac{\sqrt{35}}{8} \mathbf{S}^{44} + \frac{\sqrt{5}}{4} \mathbf{S}^{42} + \frac{3}{8} \mathbf{S}^{40} & -\frac{\sqrt{5}}{4} \mathbf{S}^{42} - \frac{1}{2} \mathbf{S}^{40} & -\frac{\sqrt{70}}{8} \mathbf{S}^{4-4} - \frac{\sqrt{10}}{8} \mathbf{S}^{4-2} & -\frac{\sqrt{35}}{8} \mathbf{S}^{43} - \frac{\sqrt{5}}{8} \mathbf{S}^{41} & -\frac{\sqrt{35}}{8} \mathbf{S}^{4-3} - \frac{3\sqrt{5}}{8} \mathbf{S}^{4-1} \\ \frac{\sqrt{5}}{4} \mathbf{S}^{42} - \frac{1}{2} \mathbf{S}^{40} & -\frac{\sqrt{5}}{4} \mathbf{S}^{42} - \frac{1}{2} \mathbf{S}^{40} & \mathbf{S}^{40} & \frac{\sqrt{10}}{4} \mathbf{S}^{4-2} & \frac{\sqrt{5}}{2} \mathbf{S}^{41} & \frac{\sqrt{5}}{2} \mathbf{S}^{4-1} \\ \frac{\sqrt{70}}{8} \mathbf{S}^{4-4} - \frac{\sqrt{10}}{8} \mathbf{S}^{4-2} & -\frac{\sqrt{70}}{8} \mathbf{S}^{4-4} - \frac{\sqrt{10}}{8} \mathbf{S}^{4-2} & \frac{\sqrt{10}}{4} \mathbf{S}^{4-2} & -\frac{\sqrt{35}}{4} \mathbf{S}^{44} + \frac{1}{4} \mathbf{S}^{40} & \frac{\sqrt{70}}{8} \mathbf{S}^{4-3} - \frac{\sqrt{10}}{8} \mathbf{S}^{4-1} & -\frac{\sqrt{70}}{8} \mathbf{S}^{43} - \frac{\sqrt{10}}{8} \mathbf{S}^{41} \\ \frac{\sqrt{35}}{8} \mathbf{S}^{43} - \frac{3\sqrt{5}}{8} \mathbf{S}^{41} & -\frac{\sqrt{35}}{8} \mathbf{S}^{43} - \frac{\sqrt{5}}{8} \mathbf{S}^{41} & \frac{\sqrt{5}}{2} \mathbf{S}^{41} & \frac{\sqrt{70}}{8} \mathbf{S}^{4-3} - \frac{\sqrt{10}}{8} \mathbf{S}^{4-1} & \frac{\sqrt{5}}{2} \mathbf{S}^{62} - \mathbf{S}^{40} & \frac{\sqrt{5}}{2} \mathbf{S}^{4-2} \\ \frac{\sqrt{35}}{8} \mathbf{S}^{4-3} - \frac{\sqrt{5}}{8} \mathbf{S}^{4-1} & -\frac{\sqrt{35}}{8} \mathbf{S}^{4-3} - \frac{3\sqrt{5}}{8} \mathbf{S}^{4-1} & \frac{\sqrt{5}}{2} \mathbf{S}^{4-1} & -\frac{\sqrt{70}}{8} \mathbf{S}^{43} - \frac{\sqrt{10}}{8} \mathbf{S}^{41} & \frac{\sqrt{5}}{2} \mathbf{S}^{4-2} & -\frac{\sqrt{5}}{2} \mathbf{S}^{42} - \mathbf{S}^{40} \end{pmatrix}. \quad (\text{S20})$$

Direct inspection of Eq. (S20) makes it evident that: (i)  $\text{tr} \mathbf{S}_{6 \times 6}^{(4)} = 0$ ; (ii) one of the eigenvalues is zero ( $\lambda_{a_0} = 0$ ); and (iii) its associated eigenvector is  $\hat{\mathbf{v}}^{(a_0)} = \frac{1}{\sqrt{3}} (1, 1, 1, 0, 0, 0)^t$ .

### S5. MINIMAL SPHERICAL DESIGNS FOR $L = 2$ AND $L = 4$ WITH ANTIPODAL SYMMETRY

Spherical designs are sets of unit vectors that fulfill Eq. (32). One can check that for any degree-2 function  $f^{(2)}(\hat{\mathbf{n}})$  with antipodal symmetry (i.e., involving  $\ell = 0$  and  $\ell = 2$  SH), the 2-design

$$\{\hat{\mathbf{n}}^\alpha\} = \{\hat{\mathbf{e}}_1, \hat{\mathbf{e}}_2, \hat{\mathbf{e}}_3\} = \{(1, 0, 0), (0, 1, 0), (0, 0, 1)\}$$

yields

$$\begin{aligned} \frac{1}{3} \sum_{\alpha=1}^3 f^{(2)}(\hat{\mathbf{n}}^\alpha) &= \frac{1}{3} \sum_{\ell=0,2} \sum_{m=-\ell}^{\ell} f^{\ell m} \mathcal{Y}_{ij}^{\ell m} (n_i^1 n_j^1 + n_i^2 n_j^2 + n_i^3 n_j^3) = \frac{1}{3} \sum_{\ell=0,2} \sum_{m=-\ell}^{\ell} f^{\ell m} \mathcal{Y}_{ij}^{\ell m} (\hat{\mathbf{e}}_1^{\otimes 2} + \hat{\mathbf{e}}_2^{\otimes 2} + \hat{\mathbf{e}}_3^{\otimes 2})_{ij} \\ &= \frac{1}{3} \sum_{\ell=0,2} \sum_{m=-\ell}^{\ell} f^{\ell m} (\mathcal{Y}_{11}^{\ell m} + \mathcal{Y}_{22}^{\ell m} + \mathcal{Y}_{33}^{\ell m}) = \frac{1}{3} \sum_{\ell=0,2} \sum_{m=-\ell}^{\ell} f^{\ell m} \mathcal{Y}_{ij}^{\ell m} \delta_{ij} = f^{00}, \end{aligned}$$

fulfilling Eq. (32). Here we used  $\mathcal{Y}_{ij}^{00} = \delta_{ij}$  that follows from Eq. (46).

Likewise, for any degree-4 function  $f^{(4)}(\hat{\mathbf{n}})$  with antipodal symmetry (involving  $\ell = 0, 2$  and  $4$  SH), the 4-design

$$\begin{aligned} \{\hat{\mathbf{n}}^\alpha\} &= \frac{1}{\sqrt{1+\varphi^2}} \{\hat{\mathbf{e}}_1 + \varphi \hat{\mathbf{e}}_2, \hat{\mathbf{e}}_2 + \varphi \hat{\mathbf{e}}_3, \hat{\mathbf{e}}_3 + \varphi \hat{\mathbf{e}}_1, \hat{\mathbf{e}}_1 - \varphi \hat{\mathbf{e}}_2, \hat{\mathbf{e}}_2 - \varphi \hat{\mathbf{e}}_3, \hat{\mathbf{e}}_3 - \varphi \hat{\mathbf{e}}_1\} \\ &= \frac{1}{\sqrt{1+\varphi^2}} \{(1, \varphi, 0), (0, 1, \varphi), (\varphi, 0, 1), (1, -\varphi, 0), (0, 1, -\varphi), (-\varphi, 0, 1)\} \end{aligned}$$

where  $\varphi = (1 + \sqrt{5})/2$ , yields

$$\begin{aligned} \frac{1}{6} \sum_{\alpha=1}^6 f^{(4)}(\hat{\mathbf{n}}^\alpha) &= \frac{1}{6} \sum_{\ell,m} f^{\ell m} \mathcal{Y}_{ijkl}^{\ell m} (n_i^1 n_j^1 n_k^1 n_l^1 + n_i^2 n_j^2 n_k^2 n_l^2 + n_i^3 n_j^3 n_k^3 n_l^3 + n_i^4 n_j^4 n_k^4 n_l^4 + n_i^5 n_j^5 n_k^5 n_l^5 + n_i^6 n_j^6 n_k^6 n_l^6) \\ &= \frac{1}{6} \sum_{\ell,m} f^{\ell m} \mathcal{Y}_{ijkl}^{\ell m} \frac{1}{(1+\varphi^2)^2} \left( (\hat{\mathbf{e}}_1 + \varphi \hat{\mathbf{e}}_2)^{\otimes 4} + (\hat{\mathbf{e}}_2 + \varphi \hat{\mathbf{e}}_3)^{\otimes 4} + \dots + (\hat{\mathbf{e}}_3 - \varphi \hat{\mathbf{e}}_1)^{\otimes 4} \right)_{ijkl} \\ &= \frac{1}{6} \sum_{\ell,m} f^{\ell m} \mathcal{Y}_{ijkl}^{\ell m} \frac{6\varphi^2}{(1+\varphi^2)^2} \left( \hat{\mathbf{e}}_1^{\otimes 4} + \hat{\mathbf{e}}_2^{\otimes 4} + \hat{\mathbf{e}}_3^{\otimes 4} + 2 \hat{\mathbf{e}}_1^{\otimes 2} \hat{\mathbf{e}}_2^{\otimes 2} + 2 \hat{\mathbf{e}}_2^{\otimes 2} \hat{\mathbf{e}}_3^{\otimes 2} + 2 \hat{\mathbf{e}}_3^{\otimes 2} \hat{\mathbf{e}}_1^{\otimes 2} \right)_{ijkl} \\ &= \frac{1}{6} \sum_{\ell,m} f^{\ell m} \frac{6}{5} \left( \mathcal{Y}_{1111}^{\ell m} + \mathcal{Y}_{2222}^{\ell m} + \mathcal{Y}_{3333}^{\ell m} + 2 (\mathcal{Y}_{1122}^{\ell m} + \mathcal{Y}_{1133}^{\ell m} + \mathcal{Y}_{2233}^{\ell m}) \right) \\ &= \frac{1}{5} \sum_{\ell,m} f^{\ell m} \mathcal{Y}_{ijkl}^{\ell m} \delta_{ij} \delta_{kl} = \frac{1}{5} \sum_{\ell,m} f^{\ell m} \mathcal{Y}_{ijkl}^{\ell m} \delta_{(ij)\delta_{kl}} = f^{00}, \end{aligned}$$

fulfilling Eq. (32). Here we used  $\varphi^2 = 1 + \varphi$ ,  $1 + \varphi^2 = \sqrt{5} \varphi$ ,  $1 + \varphi^4 = 3\varphi^2$ , as well as  $\mathcal{Y}_{ijkl}^{00} = \delta_{(ij)\delta_{kl}}$  that follows from Eq. (46), with  $\zeta(4, 0) = 5$  in Eq. (48), cf. Eqs. (S1).

## S6. SA IRREDUCIBLE DECOMPOSITION: ALL ROTATIONAL INVARIANTS

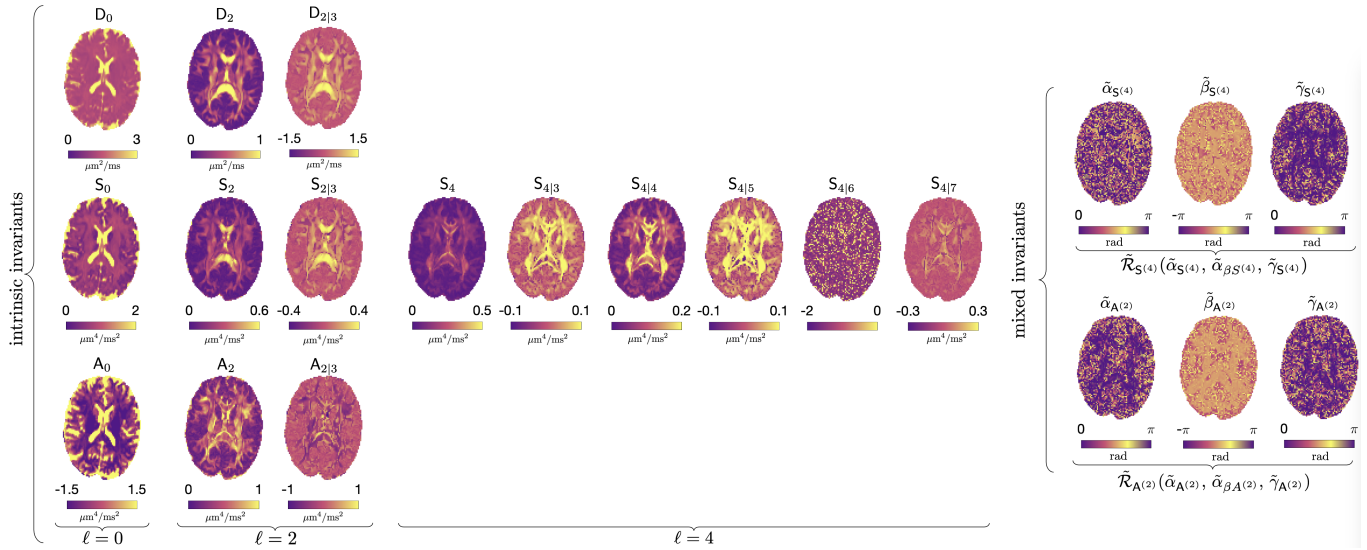


FIG. S1. RICE maps for a normal brain (33 y.o. male). Intrinsic invariants for each irreducible decomposition of  $D$ ,  $S$  and  $A$  are shown as powers of corresponding traces, to match units of  $D$  and  $C$  tensors. Combinations of just 6 intrinsic invariants (out of  $3 + 12$ ) generate all previously used model-independent dMRI contrasts, Eqs. (25)-(30). The 6 mixed invariants correspond to Euler angles of eigenframes of  $S^{(4)}$  and  $A^{(2)}$  relative to that of  $S^{(2)}$  (see text). The underlying tissue microstructure introduces correlations between invariants. For example, small relative angles  $\tilde{\beta}$  in white matter tracts exemplify the alignment of eigenframes of different representations of  $SO(3)$  with the tract.

## S7. MINIMAL PROTOCOLS VALIDATION WITH MAGNITUDE DENOISING PREPROCESSED DWI

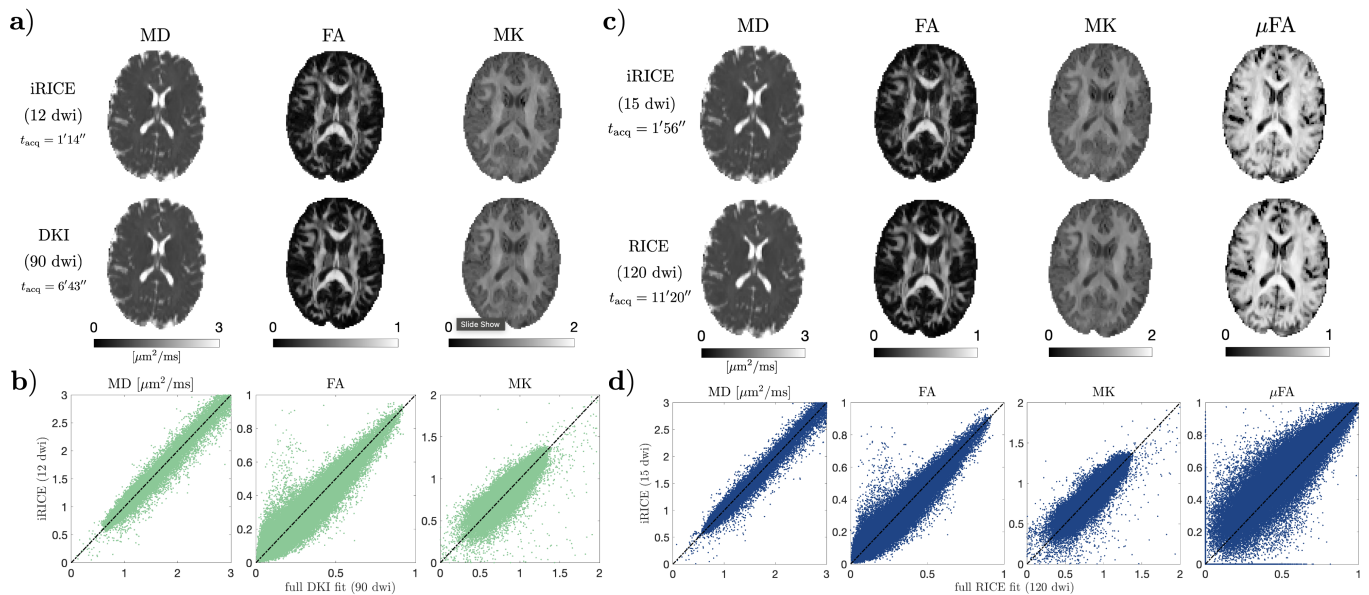


FIG. S2. Comparison of iRICE (1-2 minutes) with fully sampled acquisitions (6-11 minutes) for magnitude-denoised data. (a,c): iRICE maps (top) vs fully sampled DKI maps (bottom) for a healthy volunteer. Panels (b) and (d) show scatter plots for all brain voxels in a normal volunteer.